

Sylvester-Preconditioned Adaptive-Rank Implicit Time Integrators for Advection-Diffusion Equations with Inhomogeneous Coefficients

Hamad El Kahza^a, Jing-Mei Qiu^a, Luis Chacón^b, and William Taitano^b

^aDepartment of Mathematical Sciences, University of Delaware, Newark, DE 19716

^bTheoretical Division, Los Alamos National Laboratory, Los Alamos, NM 87545

October 28, 2024

Abstract

We consider the adaptive-rank integration of general time-dependent advection-diffusion partial differential equations (PDEs) with spatially variable coefficients. We employ a standard finite-difference method for spatial discretization coupled with diagonally implicit Runge-Kutta schemes for temporal discretization. The fully discretized scheme can be written as a generalized Sylvester equation, which we solve with an adaptive-rank algorithm structured around three key strategies: (i) constructing dimension-wise subspaces based on an extended Krylov strategy, (ii) developing an effective Averaged-Coefficient Sylvester (ACS) preconditioner to invert the reduced system for the coefficient matrix efficiently, and (iii) efficiently computing the residual of the equation without explicitly reverting to the full-rank form. The proposed approach features a computational complexity of $\mathcal{O}(Nr^2 + r^3)$, where r represents the rank during the Krylov iteration and N is the resolution in one dimension, commensurate with the constant-coefficient case [10]. We present numerical examples that illustrate the computational efficacy and complexity of our algorithm.

Keywords: Adaptive-rank, extended Krylov subspaces, implicit Runge-Kutta integrators, advection-diffusion equations, Sylvester preconditioning, matrix-equations.

1 Introduction

We propose an adaptive-rank numerical scheme for approximating the solution of the time-dependent variable-coefficient advection-diffusion equation. A challenge in existing numerical schemes is the *curse of dimensionality*, where the problem dimension d leads to exponential growth in computational complexity.

These formulations often result in large matrix systems of the form $Ax = b$, with A sparse and banded, of size N^d -by- N^d and bandwidth $\mathcal{O}(N^{d-1})$, where N is the resolution in one dimension and d is the dimensionality. Direct solvers for such systems scale in general as $\mathcal{O}(N^{3d-2})$ [3]. The complexity of unpreconditioned Conjugate Gradient (a type of Krylov method) for diffusion problems scales as $\mathcal{O}(N^{3d/2})$ [6, 19]. Multigrid-preconditioned Krylov methods may improve this scaling to $\mathcal{O}(N^d)$ [16], which is considered optimal. In all these cases, the presence of the dimension d in the exponent makes computation of the inverse matrix challenging for fine-mesh resolutions of high-dimensional problems.

Our method seeks to overcome this dimensional scaling and provide an efficient approach with a complexity of $\mathcal{O}(N)$ to solving time-dependent variable coefficient advection-diffusion partial differential equations (PDEs). In two dimensions, our approach leverages adaptive-rank approximations of matrix solutions on a tensor-product grid. Adaptive-rank techniques have proven effective in reducing the computational complexity of high-dimensional problems by representing the solution matrix as a sum of the outer products of basis vectors. Specifically, we employ a truncated singular value decomposition (SVD), such that $X = USV^\top$, where basis vectors in U and V span the solution space and determine the *rank* of the solution. The key idea is to dynamically update the basis vectors, as well as the rank (denoted as r), to maintain accuracy while minimizing computational cost.

Two primary strategies in the literature exploit low-rank structures for time-dependent PDEs: the dynamical low-rank (DLR) approximation [17, 22, 5, 8, 21] and the step-and-truncate (SAT) method, which has both explicit [18, 7, 13, 12, 14] and implicit [29, 24, 10, 23] formulations. Our work aligns with the SAT framework, where we perform temporal discretization with high-order accuracy and fully implicitly, leading to matrix differential equations to be solved at every time step. For constant coefficients, this system becomes a Sylvester equation of the form:

$$A\mathbf{X}_1 + \mathbf{X}_1B^\top = \mathbf{X}_0, \quad (1)$$

where $\mathbf{X}_1 \in \mathbb{R}^{N_1 \times N_2}$ represents the solution at time t_1 , $\mathbf{X}_0 \in \mathbb{R}^{N_1 \times N_2}$ is the initial condition at t_0 , and A and B are difference operators arising from the PDE discretization.

Krylov subspace methods have proven effective for solving Sylvester-type equations resulting from the discretization of PDEs [20, 33, 29, 25, 2]. In these methods, the solution bases are chosen from a Krylov (or Krylov-like) subspace of A and B in (1), and the original system is projected onto this reduced subspace using the Galerkin projection. To accelerate the convergence of iterative methods, various extensions of Krylov subspaces have been developed. Notably, the extended Krylov subspace [9] involving A^{-1} , B^{-1} has been applied to matrix equations in [33] and later adopted for time-dependent PDEs in [10].

While substantial progress has been made in constant-coefficient problems, systems with variable coefficients remain challenging. Discretizing such systems leads to the so-called generalized Sylvester matrix equation, of the form:

$$\sum_{i=1}^l A_i \mathbf{X}_1 B_i^\top = \mathbf{X}_0, \quad (2)$$

where A_i and B_i represent discretization operators for advection and/or diffusion terms. While these types of matrix equations can be solved by reverting them to the Kronecker form, in [26] the authors argue that, for a chosen approximation space, the Galerkin projection applied to the matrix equation consistently achieves faster convergence than the Kronecker formulation, particularly when the operators are poorly conditioned. Both analytical and numerical evidence in [26] support this claim. Furthermore, they show that the optimality of the Galerkin projection technique for Sylvester equations extends naturally to the generalized Sylvester equations. That is, regardless of the approximation space, the residual decreases as the subspaces are iteratively expanded, though the convergence rate depends significantly on the choice of subspaces, as demonstrated in [10]. Additional validation of this claim is provided in [34], where a matrix-based conjugate gradient method is compared with Galerkin projection techniques. Such results encourage the community to adopt matrix-equation-based strategies for multi-term matrix equations, rather than defaulting to Kronecker formulations.

Several methods have been proposed to solve generalized Sylvester equations iteratively directly in matrix form, either with stationary iterative techniques or Krylov methods. Stationary iterative methods [1, 32] leverage low-rank techniques to enhance efficiency, achieving computational complexity as low as $\mathcal{O}(N)$ when implemented effectively [32]. However, their effectiveness strongly depends on whether or not such a dominating operator could be correctly identified to enable a contractive iterative process. The difficulty of explicitly finding such a dominating term in a general setting was discussed in [25], which proposed using the Kronecker formulation instead.

Krylov methods have also been explored as an alternative for the solution of equations of the Sylvester and generalized Sylvester type. In [1], the authors present a series of techniques to tackle the Generalized Lyapunov equation, which is a special case of (2) where the first two terms are of Sylvester type, i.e. $A_1 = B_2 := A$, $B_1 = I_{N_2}$, and $A_2 = I_{N_1}$. Among these techniques, they discuss a low-rank projection-based scheme, in which they propose constructing extended Krylov subspaces using A , following the approach of [33], and employing a standard Krylov basis for the remaining operators. In [27], a low-rank projection-based technique is employed for systems where $N_2 \ll N_1$. The authors opt for the rational Krylov as an approximation space for the Galerkin projection of the original equation, and solve the resulting small-sized equation with either matrix-based Conjugate Gradient or a Kronecker formulation, given that N_2 is relatively small. In [15], a Krylov-based projection technique is developed for matrix equations of the form (2), where the Krylov basis construction relies on a low-rank decomposition of the operators. The resulting small generalized Sylvester matrix system is solved using the Sherman-Morrison-Woodbury formula through a series of Sylvester equation solves, which leverages the operator's low-rank structure. Finally, of particular

relevance to our study, a basis-update-and-Galerkin (BUG) DLR integrator is proposed in [23] as a low-rank GMRES preconditioner for the generalized Sylvester equation arising from advection-diffusion time-dependent problems with variable coefficients. The approach evolves the basis and the coefficient matrix in the preconditioner using BUG to provide guesses for the basis vectors and coefficient updates. The advantage of the approach is that the approximations involved in the BUG integrator are only present in the preconditioning stage, and not in the converged solution.

In contrast to existing efforts, in this work we propose an optimal implicit time integrator based on SAT adaptive-rank integrators for the variable-coefficient advection-diffusion equation. Instead of evolving the bases and coefficients simultaneously, we evolve them separately to produce an effective, inexpensive implicit solver. In particular, we iteratively construct a set of extended Krylov subspaces (for each dimension) that effectively capture the solution’s range evolution in an iterative manner. A Galerkin projection is then applied to project the full system of equations into a reduced system. The reduced system is solved using Krylov methods like GMRES, with preconditioning based on an approximated operator that transforms the generalized Sylvester equation into a regular Sylvester one, for which suitable efficient solvers exist. To assess the goodness of the solution efficiently, we propose a residual-checking mechanism that leverages the low-rank structure of solutions directly. Such procedure avoids the need to form the solution matrix for norm evaluation. The overall scheme scales as $\mathcal{O}(Nr^2 + r^3)$, with r the rank. The main innovations of our proposed algorithm are as follows:

- **Linear “1D-like” Computational Complexity:** We introduce a Krylov-based adaptive-rank algorithm for solving equations of the form (2), which arise from implicit integrators for advection-diffusion-type equations. Our method achieves *linear computational complexity* with respect to N and *quadratic complexity* with respect to r , offering a significant advantage over existing state-of-the-art adaptive-rank approaches. To the best of our knowledge, this is the first study that clearly demonstrates the optimal complexity of $\mathcal{O}(Nr^2)$ for the advection-diffusion-type equation with variable coefficients.
- **Generalized dimension-wise extended Krylov Subspaces:** We propose an averaged-coefficient approximation operator $\tilde{\mathcal{L}}$, which is instrumental not only in building dimension-wise extended Krylov subspaces, but also for preconditioning the reduced projected system. The dimension-wise Krylov subspaces are generated from multiple operators present in \mathcal{L} , $\tilde{\mathcal{L}}$ and their inverses. Such strategy is numerically demonstrated in this study to be computationally effective with rapid convergence in Krylov iterations.
- **Efficient Preconditioning Strategy:** We deploy a GMRES solver for the reduced generalized Sylvester equation from Galerkin projection (of size r^2), with an Averaging-Coefficient Sylvester (ACS) preconditioner to accelerate the Krylov convergence. The proposed preconditioner is based on a Sylvester direct solver for the averaged-coefficient approximation operator $\tilde{\mathcal{L}}$, which results in a computational complexity of $\mathcal{O}(r^3)$ (vs. the expected $\mathcal{O}(r^6)$ of a direct inversion of the Kronecker-product form of the reduced generalized Sylvester equation). This preconditioner is inspired by the recent work in [25], which employed a similar approach for the full-matrix form of the generalized Sylvester equation. A significant enhancement of the algorithm’s efficiency is demonstrated in our numerical tests.
- **Optimized solution representation and low rank residual computation:** We employ an SVD-truncated QR procedure for basis augmentation, and an SVD-truncated procedure for the intermediate solution during the Krylov iteration as often as possible. This optimizes the computational efficiency, while preserving the accuracy and structure of the solution. In addition, an efficient low-rank computation of the residual is enabled with $\mathcal{O}(r^3)$ complexity without explicitly forming the full solution on tensor-product grids. This avoids the computational cost associated with full matrix, which could otherwise spoil the linear computational complexity sought.

The structure of the rest of this paper is as follows. In Section 2, we consider the case of rank-one advection and diffusion coefficients and derive the generalized Sylvester equation that results from a finite-difference discretization in space and backward Euler in time. In Section 3, we present our adaptive-rank solution strategy, including the coefficient-averaged approximation operator, construction of extended-Krylov subspaces, preconditioning technique in solving the reduced system, and low-rank computation of the residual

norm. The extension of the technique to high-order temporal discretizations with multi-rank coefficients is provided in Appendix C. In Section 4, numerical results are presented to demonstrate the efficacy in high-order temporal convergence, adaptive rank evolution of Krylov subspaces, optimal computational complexity, as well as accelerated Krylov convergence. Finally, we conclude with a brief highlight of our proposed algorithm and outlook for future research in Section 5.

2 Problem Description and Generalized Sylvester Equation

In what follows, we refer to equations in the form of Equation (1) as the Sylvester equation, where the unknown solution matrices are operated on one dimension at a time. Additionally, we use the term *generalized* Sylvester equation to describe equations in the form of Equation (2), where each unknown solution matrix is simultaneously operated on across both dimensions.

We establish the following notation conventions based on the nature of the symbols. Lowercase Greek letters, such as $\phi(x, y)$ or $\sigma(x, y)$, denote continuous scalar fields. Uppercase bold italic Greek letters, such as $\Phi(x, y)$ or $\Sigma(x, y)$, are used for vector-valued and tensor-valued functions. Uppercase Greek letters, like Φ or Σ , represent discrete matrices arising from the discretization of continuous scalar functions or differential operators on a grid. Boldface uppercase letters, such as \mathbf{F} or \mathbf{S} , represent unknown matrix solutions or matrix right-hand sides in matrix equations. The identity matrix of size n is denoted by I_n .

We aim to solve the advection-diffusion equation:

$$\frac{\partial f}{\partial t} = \nabla_v \cdot (\Phi \cdot \nabla_v f) - \nabla_v \cdot (\Sigma f), \quad (3)$$

where $\Phi \in \mathbb{R}^{2 \times 2}$ is an isotropic diffusion tensor:

$$\Phi(x, y) = \begin{bmatrix} \phi^x(x, y) & 0 \\ 0 & \phi^y(x, y) \end{bmatrix},$$

and the advection vector $\Sigma \in \mathbb{R}^2$ is given by:

$$\Sigma(x, y) = \begin{bmatrix} \sigma^x(x, y) \\ \sigma^y(x, y) \end{bmatrix}.$$

We assume that the diffusion and advection coefficients are separable and they exhibit a low-rank structure. Specifically, the diagonal diffusion coefficients, $\phi^x(x, y)$ and $\phi^y(x, y)$, are given by:

$$\phi^x(x, y) = \sum_{i=1}^{\ell_x} \phi_i^{1,x}(x) \phi_i^{2,x}(y), \quad \phi^y(x, y) = \sum_{i=1}^{\ell_y} \phi_i^{1,y}(x) \phi_i^{2,y}(y).$$

Similarly, for the advection coefficients we have:

$$\sigma^x(x, y) = \sum_{i=1}^{k_x} \sigma_i^{1,x}(x) \sigma_i^{2,x}(y), \quad \sigma^y(x, y) = \sum_{i=1}^{k_y} \sigma_i^{1,y}(x) \sigma_i^{2,y}(y).$$

Substituting these coefficients in their separable forms into Equation (3), we obtain:

$$\begin{aligned} \frac{\partial f}{\partial t} = & \sum_{i=1}^{\ell_x} \frac{\partial}{\partial x} \left(\phi_i^{1,x}(x) \frac{\partial f(x, y)}{\partial x} \right) \phi_i^{2,x}(y) + \sum_{i=1}^{\ell_y} \phi_i^{1,y}(x) \frac{\partial}{\partial y} \left(\phi_i^{2,y}(y) \frac{\partial f(x, y)}{\partial y} \right) \\ & - \sum_{i=1}^{k_x} \frac{\partial}{\partial x} \left(\sigma_i^{1,x}(x) f(x, y) \right) \sigma_i^{2,x}(y) - \sum_{i=1}^{k_y} \sigma_i^{1,y}(x) \frac{\partial}{\partial y} \left(\sigma_i^{2,y}(y) f(x, y) \right), \end{aligned} \quad (4)$$

where, in each term, the component independent of the differentiation variable has been pulled out of the differentiation operator. Discretizing this equation using finite differences in space and an implicit method in time naturally leads to a multi-term matrix differential equation where the unknown solution is acted

upon from both directions in each term and at the same time. Numerous strategies have been proposed in the literature to solve such equations, most notably the recent work by Palitta and Simoncini in [25]. In this work, inspired by their preconditioning technique [25], we further exploit the low-rank structure of the solution and design a projection-based algorithm with an optimal scaling of $\mathcal{O}(Nr^2)$, i.e. a linear scaling with respect to the resolution N per spatial dimension, and quadratic scaling with respect to the rank r .

2.1 Generalized Sylvester Equation from Implicit Discretization of Advection-Diffusion

To simplify the presentation, we assume rank-one advection and diffusion coefficients, i.e.:

$$\begin{aligned}\phi^x &= \phi^{1,x}(x)\phi^{2,x}(y), & \phi^y &= \phi^{1,y}(x)\phi^{2,y}(y)^\top, \\ \sigma^x &= \sigma^{1,x}(x)\sigma^{2,x}(y), & \sigma^y &= \sigma^{1,y}(x)\sigma^{2,y}(y).\end{aligned}$$

Thus, Equation (4) simplifies to:

$$\begin{aligned}\frac{\partial f}{\partial t} &= \underbrace{\frac{\partial}{\partial x} \left(\phi^{1,x}(x) \frac{\partial f(x,y)}{\partial x} \right) \phi^{2,x}(y) + \phi^{1,y}(x) \frac{\partial}{\partial y} \left(\phi^{2,y}(y) \frac{\partial f(x,y)}{\partial y} \right)}_{\text{diffusion}} \\ &\quad - \underbrace{\frac{\partial}{\partial x} (\sigma^{1,x}(x)f(x,y)) \sigma^{2,x}(y) - \sigma^{1,y}(x) \frac{\partial}{\partial y} (\sigma^{2,y}(y)f(x,y))}_{\text{advection}}.\end{aligned}\tag{5}$$

We discretize this equation in a two-dimensional tensor-product spatial grid with N_1 and N_2 grid points in the x - and y - directions, respectively. The grid points in the x - direction are denoted as x_i for $i = 0, \dots, N_1 - 1$, and similarly for the y -direction. We consider the point-wise multiplication of the advection and diffusion coefficients in the discrete by setting:

$$\begin{aligned}\Phi_1 &= \text{diag}(\phi^{1,y}(x_i)), \Sigma_1 = \text{diag}(\sigma^{1,y}(x_i)), & i &= 0, \dots, N_1 - 1, \\ \Phi_2 &= \text{diag}(\phi^{2,x}(y_j)), \Sigma_2 = \text{diag}(\sigma^{2,x}(y_j)), & j &= 0, \dots, N_2 - 1.\end{aligned}$$

We approximate the spatial derivative with a three-point stencil, and obtain the following matrix differential equation for \mathbf{F} , for which its (i, j) entry $F_{i,j}$ corresponds to the approximation of $f(x_i, y_j)$:

$$\frac{\partial \mathbf{F}}{\partial t} = \underbrace{D_{xx}^\Phi \mathbf{F} \Phi_2^\top + \Phi_1 \mathbf{F} D_{yy}^\Phi}^{\text{diffusion}} - \underbrace{D_x^\Sigma \mathbf{F} \Sigma_2^\top - \Sigma_1 \mathbf{F} D_y^\Sigma}^{\text{advection}}.\tag{6}$$

Here, $D_{xx}^\Phi, D_{yy}^\Phi, D_x^\Sigma, D_y^\Sigma$ represent compositions of difference operators with pointwise multiplication operators. See Appendices A and B for more details. For notational simplicity, let

$$T_1 = D_{xx}^\Phi, \quad T_2 = D_{yy}^\Phi, \quad T_3 = -D_x^\Sigma, \quad T_4 = -D_y^\Sigma.\tag{7}$$

Equation (6) can be written compactly as:

$$\frac{\partial \mathbf{F}}{\partial t} = \mathcal{L}(\mathbf{F}),\tag{8}$$

where the right-hand side induces the following mapping:

$$\mathcal{L} : \mathbf{F} \mapsto T_1 \mathbf{F} \Phi_2^\top + \Phi_1 \mathbf{F} T_2^\top + T_3 \mathbf{F} \Sigma_2^\top + \Sigma_1 \mathbf{F} T_4^\top.\tag{9}$$

We consider first a backward Euler implicit treatment of the temporal component of the matrix differential equation (8), which gives the following generalized Sylvester equation:

$$\mathbf{F}_1 - \Delta t \mathcal{L}(\mathbf{F}_1) = \mathbf{F}_0,\tag{10}$$

with the residual equation defined as:

$$\mathbf{R}_{\mathcal{L}} = \mathbf{F}_1 - \Delta t \mathcal{L}(\mathbf{F}_1) - \mathbf{F}_0 = \mathbf{0}.\tag{11}$$

An iterative solver naturally updates the solution \mathbf{F}_1 until the residual is sufficiently small under a suitable norm.

If we vectorize the right-hand side using the Kronecker product identity, $\text{vec}(\mathbf{A}\mathbf{F}\mathbf{B}^\top) = (\mathbf{B} \otimes \mathbf{A})\text{vec}(\mathbf{F})$, the second term with a factor of Δt in (10) can be written as a matrix-vector multiplication of the form:

$$\mathbf{F} \mapsto \left[\underbrace{(\Phi_2 \otimes T_1) + (T_2 \otimes \Phi_1) + (\Sigma_2 \otimes T_3) + (T_4 \otimes \Sigma_1)}_{\in \mathbb{R}^{N_1 N_2 \times N_1 N_2}} \right] \text{vec}(\mathbf{F}), \quad (12)$$

The Kronecker form yields a linear system $Ax = b$, which can be solved either directly or iteratively. The Kronecker approach offers valuable theoretical insights into the relationship between the Kronecker structure and the constructed Krylov basis, a connection exploited in the context of Sylvester equations in [20, 23]. We note that, based on the discussion in [26] on the advantages of the dimension-wise Krylov subspaces projection approach vs. the Kronecker formulation, we choose to adopt the former approach for better computational efficiency and iterative convergence.

3 Krylov-Based Adaptive-Rank Solver for Generalized Sylvester Equation

We propose an adaptive-rank algorithm for the generalized Sylvester equation (10). We assume a low-rank factorization of the initial condition, $\mathbf{F}_0 \in \mathbb{R}^{N_1 \times N_2}$, which evolves to an updated solution $\mathbf{F}_1 \in \mathbb{R}^{N_1 \times N_2}$ at time $t^{(1)} = t^{(0)} + \Delta t$ also in the low-rank format. We represent this as:

$$\mathbf{F}_0 = U_0 S_0 V_0^\top \xrightarrow{\text{evolve in time}} \mathbf{F}_1 = U_1 S_1 V_1^\top, \quad (13)$$

where $U_0 \in \mathbb{R}^{N_1 \times r_0}$, $V_0 \in \mathbb{R}^{N_2 \times r_0}$, $U_1 \in \mathbb{R}^{N_1 \times r_1}$, and $V_1 \in \mathbb{R}^{N_2 \times r_1}$ are orthonormal bases for their respective dimensions, and $S_0 \in \mathbb{R}^{r_0 \times r_0}$ and $S_1 \in \mathbb{R}^{r_1 \times r_1}$ are diagonal matrices with singular values at the corresponding times. Our method involves constructing the bases U_1 and V_1 and then projecting the original equation to determine the coefficients of S_1 . A key aspect of the proposed adaptive-rank approach is that we do not form the full solutions explicitly. Instead, we seek bases in a dimension-by-dimension manner and then use them to perform Galerkin projection, resulting in a reduced system for the matrix of coefficients S_1 . An SVD truncation procedure is then applied to update the orthonormal basis sets and realize an efficient low-rank representation of the updated solution. Key questions for solving the *generalized* Sylvester equation in the form of (10) that we address in this paper include:

- How do we choose suitable subspaces to build U_1 and V_1 from U_0 and V_0 ?
- How can we solve the reduced equation for S_1 efficiently?
- How can we check the residual of the generalized Sylvester equation without forming the matrices explicitly?

Our main innovation involves leveraging an approximate operator denoted by $\tilde{\mathcal{L}}$ (which is of the Sylvester form) to the original operator \mathcal{L} in (9). $\tilde{\mathcal{L}}$ approximates the diagonal matrices Φ_i and Σ_i representing pointwise multiplication of diffusion and advection coefficients, respectively, by scaled identities. This approximation not only allows us to construct dimension-wise Krylov bases U_1 and V_1 effectively and efficiently, but also enables effective preconditioning in the spirit of [25]. Then we project Equation (10) onto the Krylov bases, resulting in a reduced system for the coefficient matrix S_1 . In this section, we introduce the main steps of our proposed algorithm as illustrated in Figure 1, highlighting the intuition behind our design and innovations along the way. Section 3.1 covers the construction of the approximated operator $\tilde{\mathcal{L}}$. Section 3.2 discusses the dimension-wise basis construction related to step 1 of the flowchart. In Section 3.3, we present the reduced equation for the matrix of coefficients S_1 and introduce our ACS preconditioner, corresponding to step 2 (i) in the flowchart. Lastly, Section 3.4 outlines the solution truncation mechanism and the residual computation, as described in steps 2(ii)-(iii) of the flowchart.

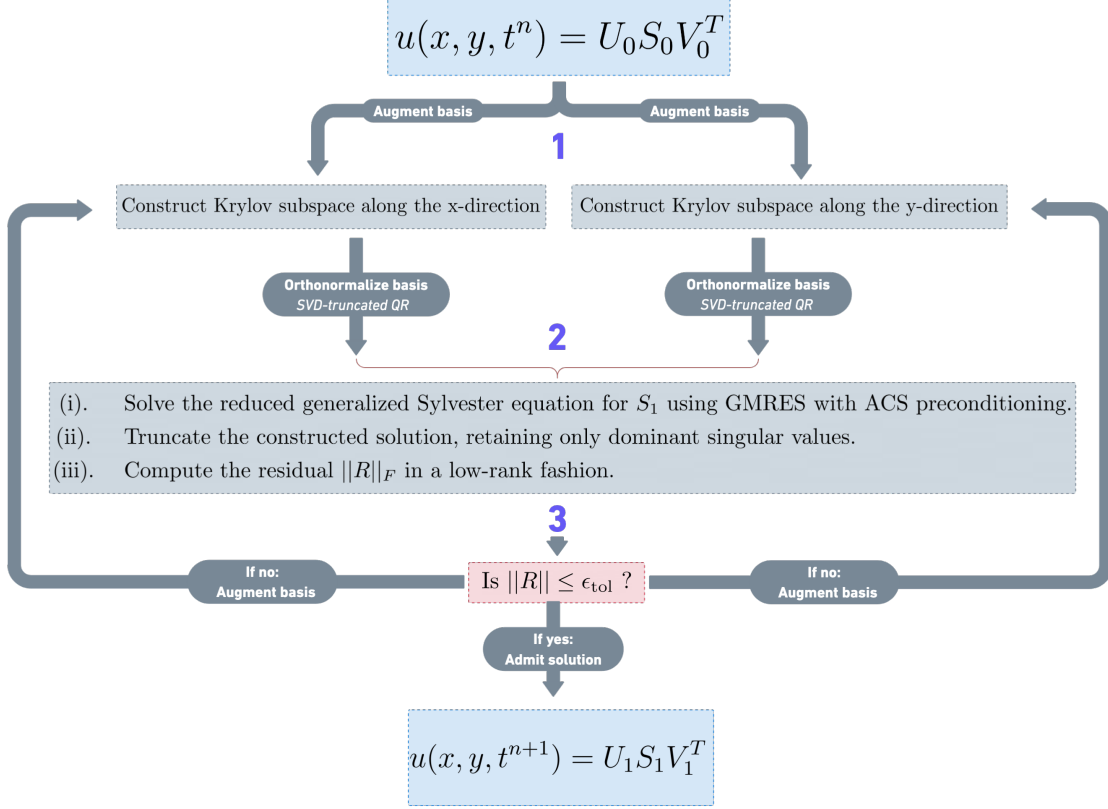


Figure 1: Flow-chart of the proposed implicit adaptive-rank algorithm for a generalized Sylvester equation.

3.1 Averaged-coefficient Approximate operator $\tilde{\mathcal{L}}$

Our approach incorporates ideas from [25] and [10] to construct an approximate operator $\tilde{\mathcal{L}}$ and efficiently solve the time-dependent inhomogeneous advection-diffusion equation using a projection-based adaptive-rank integration framework. The approximated operator $\tilde{\mathcal{L}}$ serves two purposes: (i) constructing the solution bases U_1 and V_1 as extended Krylov subspaces, and (ii) preconditioning the solution of the coefficient matrix S_1 . We first construct a basis informed by both the original operator \mathcal{L} and the approximate operator $\tilde{\mathcal{L}}$ (defined below). Secondly, we derive a corresponding projected (reduced) system that we solve iteratively using GMRES with a preconditioner derived from $\tilde{\mathcal{L}}$.

We seek an approximation to operator (9) that retains its spectral content and is easier to invert. As proposed in [25], the diagonal operators can be approximated by scaling with an identity matrix, where the scaling factor is the average of the diagonal entries. For instance, let $\Phi_i \approx \alpha_i I$ and $\Sigma_i \approx \gamma_i I$, where α_i and γ_i are the average of the diagonal entries of Φ_i and Σ_i , respectively. This approximation yields the following mapping:

$$\tilde{\mathcal{L}} : \mathbf{F} \mapsto (\alpha_2 T_1 + \gamma_2 T_3) \mathbf{F} + \mathbf{F} (\alpha_1 T_2 + \gamma_1 T_4)^\top. \quad (14)$$

A backward Euler temporal discretization using (14) yields the residual equation:

$$\mathbf{R}_{\tilde{\mathcal{L}}} = \mathbf{F}_1 - \Delta t \tilde{\mathcal{L}}(\mathbf{F}_1) - \mathbf{F}_0 = \mathbf{0},$$

which leads to the Sylvester equation:

$$(A_1 + A_3) \mathbf{F}_1 + \mathbf{F}_1 (A_2 + A_4)^\top = \mathbf{F}_0. \quad (15)$$

Here:

$$A_1 = \left(\frac{1}{4}I - \Delta t \alpha_2 T_1 \right) \quad A_3 = \left(\frac{1}{4}I - \Delta t \gamma_2 T_3 \right), \quad P_1 = A_1 + A_3, \quad (16)$$

$$A_2 = \left(\frac{1}{4}I - \Delta t \alpha_1 T_2 \right) \quad A_4 = \left(\frac{1}{4}I - \Delta t \gamma_1 T_4 \right), \quad P_2 = A_2 + A_4. \quad (17)$$

The solution to Equation (15) is an approximation to that of (10), but it can be efficiently computed using low-rank approximations [10, 33, 31, 30]. It can therefore be exploited as a viable preconditioner for a GMRES iterative solution of the generalized Sylvester equation (10). This was done in [25] with $\mathcal{O}(N^3)$ computational complexity. In this work, we extend this approach by performing a Galerkin projection of both the original operator \mathcal{L} and its approximation $\tilde{\mathcal{L}}$ on the low-rank bases before solving the generalized Sylvester equation with GMRES. This reduces the problem to a lower-dimensional subspace, where preconditioning can be applied more effectively on a smaller problem with $\mathcal{O}(r^3)$ complexity, resulting in an overall computational complexity of $\mathcal{O}(Nr^2 + r^3)$.

3.2 Basis Construction

We begin by defining the generalized Krylov subspaces used for our basis construction at the m th iteration:

$$\kappa_m(M_1, \dots, M_l, U) = [U, \underbrace{M_1 U, \dots, M_l U}_{\text{1st augmentation}}, \dots, \underbrace{M_1^{m+1} U, \dots, M_l^{m+1} U}_{\text{mth augmentation}}]. \quad (18)$$

where M_1, \dots, M_l are operators of interest and their inverses arising in our generalized Sylvester equation, and l is the number of operators used for each basis augmentation step.

In our setting, the basis construction involves several operators from the original generalized Sylvester equation (10) and its approximation (15). We first consider the action of the diagonal operators, which have been averaged to obtain the approximated operators, Φ_1 , Σ_1 , Φ_2 , and Σ_2 . We have found that including these matrices is crucial for accelerating convergence. Using these operators, we construct a standard Krylov subspace. Additionally, we use the inverse operators from the approximated operators $A_{1:4}$ in (16)-(17) to form an inverted Krylov subspace. Finally, we construct dimension-wise extended Krylov subspaces for the approximated operator $\tilde{\mathcal{L}}$ using P_1 and P_2 . The reasoning behind these choices of operators for subspace construction is as follows. Following [10], we construct an extended Krylov subspace in the x -direction for the approximated Sylvester equation (15) using P_1 and its inverse. To further enrich the basis, we include the inverses of the individual operators A_1 and A_3 , as they may contain information not captured by the inverse of P_1 . This carefully chosen set of operators results in a compact representation of the solution matrix, enriching the basis while keeping its dimension small.

Combining these, we define the extended Krylov subspaces in the x direction as follows:

$$\kappa_m(P_1, P_1^{-1}, A_1^{-1}, A_3^{-1}, \Phi_1, \Sigma_1, U_0),$$

We then apply an SVD-truncated QR, as outlined in Algorithm 1, to orthogonalize the subspace and obtain a basis $U_1^{(m)} \in \mathbf{R}^{N_1 \times r_x^{(m)}}$ and remove vectors that are closely linearly dependent. By leveraging the rank-revealing property of SVD, only those basis associated with significant singular values are retained. The same procedures are applied to the y -direction to obtain $V_1^{(m)} \in \mathbf{R}^{N_2 \times r_y^{(m)}}$. For notational simplicity, we will omit the superscript (m) from now on, understanding that $U_1 \in \mathbf{R}^{N_1 \times r_x}$ and $V_1 \in \mathbf{R}^{N_2 \times r_y}$ refer to the bases of the Krylov subspaces at the m th iteration. This truncated orthonormalization strategy is particularly advantageous when the underlying processes (diffusion or advection) are weak. In such cases, the approximated coefficient matrices contribute minimally, reducing the impact of the operator application and enabling further basis truncation.

These constructed orthonormal bases will be used to represent the solution in the approximation subspace. The coefficients composing the linear combination of these basis vectors will be obtained by projecting the corresponding generalized Sylvester equation and evolving the matrix of coefficients S_1 .

Algorithm 1: SVD-truncated QR, $\mathcal{T}_{\epsilon_\kappa}$

Input: Krylov Subspace κ_m ; Tolerance ϵ_κ .

Output: Truncated bases Q .

- (1) Compute the reduced QR decomposition: $\{Q, R\} = \text{QR}(\kappa_m)$;
 - (2) Perform reduced SVD decomposition: $T_1 \tilde{R} T_2 = \text{SVD}(R)$, where $\tilde{R} = \text{diag}(\sigma_j)$;
 - (3) Identify the last index r such that $\sigma_r > \epsilon_\kappa$;
 - (4) Update the basis vectors: $Q \leftarrow Q T_1(:, 1:r)$;
-

3.3 Solving for the Matrix of Coefficients, S_1 : ACS-preconditioned GMRES

With the orthonormal bases $U_1 \in \mathbb{R}^{N_1 \times r_x}$ and $V_1 \in \mathbb{R}^{N_2 \times r_y}$ at hand, we perform a Galerkin projection to derive a reduced generalized Sylvester equation for the matrix $S_1 \in \mathbb{R}^{r_x \times r_y}$. The reduced Sylvester equation for S_1 arises from projecting the residual via the Galerkin condition $U_1^\top \mathbf{R}_{\mathcal{L}} V_1 = 0$, which yields:

$$\mathbf{S}_1 - \Delta t \left(\tilde{T}_1 \mathbf{S}_1 \tilde{\Phi}_2 + \tilde{\Phi}_1 \mathbf{S}_1 \tilde{T}_2^\top + \tilde{T}_3 \mathbf{S}_1 \tilde{\Sigma}_2 + \tilde{\Sigma}_1 \mathbf{S}_1 \tilde{T}_4^\top \right) = \tilde{\mathbf{B}}_1, \quad \text{with} \quad \tilde{\mathbf{B}}_1 = (U_1^\top U_0) S_0 (V_1^\top V_0)^\top. \quad (19)$$

This matrix-based equation is equivalent to the classical Kronecker formulation:

$$\underbrace{\left[I_{r_x r_y \times r_x r_y} - \Delta t \left(\tilde{\Phi}_2 \otimes \tilde{T}_1 + \tilde{T}_2 \otimes \tilde{\Phi}_1 + \tilde{\Sigma}_2 \otimes \tilde{T}_3 + \tilde{T}_4 \otimes \tilde{\Sigma}_1 \right) \right]}_{\mathcal{A}} \text{vec}(\mathbf{S}_1) = \text{vec}(\tilde{\mathbf{B}}_1). \quad (20)$$

The projected operators are defined as follows:

$$\begin{aligned} \tilde{T}_1 &= U_1^\top T_1 U_1, & \tilde{T}_3 &= U_1^\top T_3 U_1, & \tilde{\Phi}_1 &= U_1^\top \Phi_1 U_1, & \tilde{\Sigma}_1 &= U_1^\top \Sigma_1 U_1, \\ \tilde{T}_2 &= V_1^\top T_2 V_1, & \tilde{T}_4 &= V_1^\top T_4 V_1, & \tilde{\Phi}_2 &= V_1^\top \Phi_2 V_1, & \tilde{\Sigma}_2 &= V_1^\top \Sigma_2 V_1. \end{aligned}$$

Solving Equation (19) using the Kronecker formulation $\text{Avec}(\mathbf{S}_1) = \text{vec}(\tilde{\mathbf{B}}_1)$ with a direct solver requires a complexity of $\mathcal{O}(r^6)$, where $r = \max(r_x, r_y)$, which may be too expensive even for moderate r -values. Instead, we solve this equation using preconditioned GMRES, where the operator-times-vector operation is performed using a matrix-based strategy, with complexity $\mathcal{O}(r^3)$. This is possible due to the Kronecker structure of our operator, yielding the equivalence between (19) and (20). Given a vector $s_k = \text{vec}(\mathbf{S}_k)$, the product of the matrix \mathcal{A} times a vector s_k is organized as follows:

1. Given s_k , reshape to $\mathbf{S}_k \in \mathbb{R}^{r_x \times r_y}$, such that $\text{vec}(\mathbf{S}_k) = s_k$.
2. Compute $\hat{\mathbf{Z}}_k \leftarrow \mathbf{S}_k - \Delta t \left(\tilde{T}_1 \mathbf{S}_k \tilde{\Phi}_2 + \tilde{\Phi}_1 \mathbf{S}_k \tilde{T}_2^\top + \tilde{T}_3 \mathbf{S}_k \tilde{\Sigma}_2 + \tilde{\Sigma}_1 \mathbf{S}_k \tilde{T}_4^\top \right)$, with complexity $\mathcal{O}(r^3)$.
3. Reshape $\hat{z}_k = \text{vec}(\hat{\mathbf{Z}}_k)$.

The computational complexity of the GMRES solve also depends crucially on the total number of iterations needed to invert the linear system. To bound the number of GMRES iterations with respect to the basis dimension (rank) r , we require effective preconditioning, such that the eigenvalues of the preconditioned matrix are clustered and the number of iterations becomes independent of the system size r [4]. Here, we propose a (left) preconditioner \mathcal{P} such that the system:

$$\mathcal{P}^{-1} \text{Avec}(\mathbf{S}_1) = \mathcal{P}^{-1} \text{vec}(\tilde{\mathbf{B}}_1). \quad (21)$$

is well conditioned. The preconditioning step in GMRES requires applying \mathcal{P}^{-1} to an arbitrary vector provided by the algorithm.

For fast GMRES convergence, \mathcal{P} should approximate the left-hand side of Equation (20) well while being easier to invert than the original system. Here, we consider $\mathcal{P} = I_{r_y} \otimes \tilde{P}_1 + \tilde{P}_2 \otimes I_{r_x}$ arising from the Galerkin projection of Equation (15). In particular, let U_1 and V_1 be the orthonormal basis for the generalized Krylov subspaces, and let $\tilde{P}_1 = U_1^\top P_1 U_1$ and $\tilde{P}_2 = V_1^\top P_2 V_1$, then

$$\mathcal{P} : \mathbf{S} \mapsto \tilde{P}_1 \mathbf{S} + \mathbf{S} \tilde{P}_2^\top. \quad (22)$$

To compute $\mathcal{P}^{-1}\hat{z}_k = z_k$, we solve the corresponding Sylvester equation:

$$\tilde{P}_1 \mathbf{Z}_k + \mathbf{Z}_k \tilde{P}_2^\top = \hat{\mathbf{Z}}_k,$$

where $z_k = \text{vec}(\mathbf{Z}_k) \in \mathbb{R}^{r_x r_y}$. Specific steps are as follows:

1. Given \hat{z}_k , reshape to $\hat{\mathbf{Z}}_k \in \mathbb{R}^{r_x \times r_y}$, such that $\text{vec}(\hat{\mathbf{Z}}_k) = \hat{z}_k$.
2. Solve $\mathcal{P}_1 \mathbf{Z}_k + \mathbf{Z}_k \mathcal{P}_2^\top = \hat{\mathbf{Z}}_k$ with complexity $\mathcal{O}(r^3)$, for example with the Bartels Stewart algorithm [11].
3. Reshape $z_k = \text{vec}(\mathbf{Z}_k)$.

The proposed preconditioner effectively bounds the number of GMRES iterations required to solve Equation (19) independently of r , as will be shown later in this study, rendering the computational complexity of the S matrix solve as $\mathcal{O}(r^3)$, much better than the expected $\mathcal{O}(r^6)$ scaling of a naïve implementation of GMRES.

3.4 Truncation, Efficient Residual Computation, and Algorithm Flowchart

At the end of each iteration, we need to compute the residual to accept or reject the low-rank approximation from Krylov subspaces. This process should take advantage of the low-rank representation of the solution while avoiding forming the residual on the full grid.

Once the solution $\mathbf{F}_1 = U_1 S_1 V_1^\top$ is obtained, we apply truncation to control rank growth and reduce the residual computational load. Since S_1 from the GMRES solve is not necessarily diagonal, we follow the approach in [14] to convert it into a singular value form (also scaling as $\mathcal{O}(r^3)$) and discard singular values below a threshold ϵ . The truncation results in a solution $\mathbf{F}_1 = U_1 S_1 V_1^\top$, with $U_1 \in \mathbb{R}^{N_1 \times r_1}$, $V_1 \in \mathbb{R}^{N_2 \times r_1}$, and $S_1 \in \mathbb{R}^{r_1 \times r_1}$, with $r_1 \leq \min(r_x, r_y)$. This procedure is summarized in Algorithm 2.

Following a similar procedure to [10], we devise a cost-effective way to compute the residual using the identity:

$$\begin{aligned} \|\mathbf{R}_{\mathcal{L}}\| &= \|\mathbf{F}_1 - \Delta t \mathcal{L}(\mathbf{F}_1) - \mathbf{F}_0\| \\ &= \left\| R_U \underbrace{\begin{bmatrix} S_1 - \tilde{B}_1 & \mathbf{0} & \mathbf{0} & \mathbf{0} & \mathbf{0} \\ \mathbf{0} & -\Delta t S_1 & \mathbf{0} & \mathbf{0} & \mathbf{0} \\ \mathbf{0} & \mathbf{0} & -\Delta t S_1 & \mathbf{0} & \mathbf{0} \\ \mathbf{0} & \mathbf{0} & \mathbf{0} & -\Delta t S_1 & \mathbf{0} \\ \mathbf{0} & \mathbf{0} & \mathbf{0} & \mathbf{0} & -\Delta t S_1 \end{bmatrix}}_{\in \mathbb{R}^{5r_1 \times 5r_1}} R_V^\top \right\| \\ &= \left\| R_U \begin{bmatrix} S_1 - \tilde{B}_1 & \mathbf{0} \\ \mathbf{0} & -\Delta t (I_{\mathcal{R}_{\text{ranks}}} \otimes S_1) \end{bmatrix} R_V^\top \right\| \leq \epsilon_{\text{tol}}, \end{aligned}$$

where $\mathcal{R}_{\text{ranks}} = \ell_x + k_x + \ell_y + k_y$ is the total rank number of the advection and diffusion coefficients, and where R_U and R_V are the upper triangular matrices arising from the following QR decomposition:

$$\begin{aligned} \{-, R_U\} &= \text{QR}([U_1 \quad T_1 U_1 \quad \Phi_1 U_1 \quad T_3 U_1 \quad \Sigma_1 U_1]), \\ \{-, R_V\} &= \text{QR}([V_1 \quad \Phi_2 V_1 \quad T_2 V_1 \quad \Sigma_2 V_1 \quad T_4 V_1]), \end{aligned} \tag{23}$$

where the orthogonal columns from the decomposition are ignored. The above residual result follows because, if $\mathbf{F}_0 = U_0 S_0 V_0^\top$ (where $U_0 \in \mathbb{R}_0^{N \times r_0}$ and $V_0 \in \mathbb{R}_0^{N \times r_0}$ have orthonormal columns) then, since U_1 and V_1 contain U_0 and V_0 , respectively, we have $U_1 (U_1)^\top \mathbf{F}_0 V_1 (V_1)^\top = \mathbf{F}_0$.

3.5 Generalization to Multi-rank Coefficients

We generalize next the adaptive-rank approach from rank-one advection and diffusion coefficients to the multi-rank case, using backward Euler. The corresponding pseudo-algorithm is presented in Algorithm

Algorithm 2: Truncated SVD, \mathcal{T}_ϵ

Input: Bases U, V ; matrix of coefficients S ; Tolerance ϵ .

Output: Truncated bases \tilde{U}, \tilde{V} ; truncated singular values \tilde{S} .

- (1) Perform reduced SVD decomposition: $T_1 \tilde{S} T_2 = \text{SVD}(S)$, where $\tilde{S} = \text{diag}(\sigma_j)$;
 - (2) Identify the last index r_1 such that $\sigma_{r_1}/\|S\| > \epsilon$;
 - (3) Update matrix of singular values: $\tilde{S} \leftarrow \tilde{S}(1:r_1, 1:r_1)$;
 - (4) Update left singular vectors: $\tilde{U} \leftarrow UT_1(:, 1:r_1)$;
 - (5) Update the right singular vectors: $\tilde{V} \leftarrow VT_2(:, 1:r_1)$;
-

3. High-order temporal discretizations are considered later in this study. Discretization of the multi-rank advection-diffusion equation yields a multi-term generalized Sylvester equation of the form:

$$\mathbf{F}_1 - \Delta t \underbrace{\left(\sum_{i=1}^{\ell_x} T_{1,i} \mathbf{F}_1 \Phi_i^{2,x\top} + \sum_{j=1}^{\ell_y} \Phi_j^{1,y} \mathbf{F}_1 T_{2,j}^\top + \sum_{k=1}^{k_x} T_{3,k} \mathbf{F}_1 \Sigma_k^{2,x\top} + \sum_{l=1}^{k_y} \Sigma_l^{1,y} \mathbf{F}_1 T_{4,l}^\top \right)}_{\mathcal{L}(\mathbf{F}_1)} = \mathbf{F}_0. \quad (24)$$

As before, we find $\tilde{\mathcal{L}}$ by averaging the diagonal terms $(\Phi_i^{2,x}, \Phi_j^{1,y}, \Sigma_k^{2,x}, \Sigma_l^{1,y})$ from (24) as follows:

$$\alpha_{x,i} = \text{average}(\Phi_i^{2,x}), \quad \alpha_{y,j} = \text{average}(\Phi_j^{1,y}), \quad \gamma_{x,k} = \text{average}(\Sigma_k^{2,x}), \quad \gamma_{y,l} = \text{average}(\Sigma_l^{1,y}), \quad (25)$$

to arrive at the approximated Sylvester equation:

$$P_1 \mathbf{F}_1 + \mathbf{F}_1 P_2^\top = \mathbf{F}_0, \quad (26)$$

where

$$P_1 = \sum_{i=1}^{\ell_x} A_{1,i} + \sum_{k=1}^{k_x} A_{3,k} = \sum_{i=1}^{\ell_x} \left(\frac{1}{\mathcal{R}_{\text{ranks}}} I_{N_1} - \Delta t \alpha_{x,i} T_{1,i} \right) + \sum_{k=1}^{k_x} \left(\frac{1}{\mathcal{R}_{\text{ranks}}} I_{N_1} - \Delta t \gamma_{x,k} T_{3,k} \right),$$

$$P_2 = \sum_{j=1}^{\ell_y} A_{2,j} + \sum_{l=1}^{k_y} A_{4,l} = \sum_{j=1}^{\ell_y} \left(\frac{1}{\mathcal{R}_{\text{ranks}}} I_{N_2} - \Delta t \alpha_{y,j} T_{2,j} \right) + \sum_{l=1}^{k_y} \left(\frac{1}{\mathcal{R}_{\text{ranks}}} I_{N_2} - \Delta t \gamma_{y,l} T_{4,l} \right).$$

The bases U_1 and V_1 are constructed from orthonormalization of dimension-wise generalized Krylov subspaces from equations (24) and (26) as follows:

$$U_1 = \mathcal{T}_{\epsilon_\kappa} \left(\kappa_m \left(P_1, P_1^{-1}, A_{1,1:\ell_x}^{-1}, A_{3,1:k_x}^{-1}, \Phi_{1:\ell_y}^{1,y}, \Sigma_{1:k_y}^{1,y}, U_0 \right) \right), \quad (27)$$

$$V_1 = \mathcal{T}_{\epsilon_\kappa} \left(\kappa_m \left(P_2, P_2^{-1}, A_{2,1:\ell_y}^{-1}, A_{4,1:k_y}^{-1}, \Phi_{1:\ell_x}^{2,x}, \Sigma_{1:k_x}^{2,x}, V_0 \right) \right), \quad (28)$$

In the multi-rank setting, after a Galerkin projection $U^\top \mathbf{R}_{\mathcal{L}} V = 0$, we obtain a generalized Sylvester equation similar to (29) for the matrix of coefficients S_1 :

$$\mathbf{S}_1 - \Delta t \left(\sum_{i=1}^{\ell_x} \tilde{T}_{1,i} \mathbf{S}_1 \tilde{\Phi}_i^{2,x\top} + \sum_{j=1}^{\ell_y} \tilde{\Phi}_j^{1,y} \mathbf{S}_1 \tilde{T}_{2,j}^\top + \sum_{k=1}^{k_x} \tilde{T}_{3,k} \mathbf{S}_1 \tilde{\Sigma}_k^{2,x\top} + \sum_{l=1}^{k_y} \tilde{\Sigma}_l^{1,y} \mathbf{S}_1 \tilde{T}_{4,l}^\top \right) = \tilde{\mathbf{B}}_1 \quad (29)$$

where the projected operators are analogous to those defined in the rank-one case.

Afterwards, as before, we solve (29) for the S_1 matrix using preconditioned GMRES. The preconditioner is constructed by a Galerkin projection $U^\top \mathbf{R}_{\mathcal{L}} V = 0$, to find the projected Sylvester equation:

$$\tilde{P}_1 \mathbf{S} + \mathbf{S} \tilde{P}_2^\top = \tilde{B}_1, \quad (30)$$

with:

$$\begin{aligned}\tilde{P}_1 &= \sum_{i=1}^{\ell_x} \underbrace{\left(\frac{1}{\mathcal{R}_{\text{ranks}}} I_{r_x} - \Delta_t \alpha_{x,i} \tilde{T}_{1,i} \right)}_{\tilde{A}_{1,i}} + \sum_{k=1}^{k_x} \underbrace{\left(\frac{1}{\mathcal{R}_{\text{ranks}}} I_{r_x} - \Delta_t \gamma_{x,k} \tilde{T}_{3,k} \right)}_{\tilde{A}_{3,k}}, \\ \tilde{P}_2 &= \sum_{j=1}^{\ell_y} \underbrace{\left(\frac{1}{\mathcal{R}_{\text{ranks}}} I_{r_y} - \Delta_t \alpha_{y,j} \tilde{T}_{2,j} \right)}_{\tilde{A}_{2,j}} + \sum_{l=1}^{k_y} \underbrace{\left(\frac{1}{\mathcal{R}_{\text{ranks}}} I_{r_y} - \Delta_t \gamma_{y,l} \tilde{T}_{4,l} \right)}_{\tilde{A}_{4,l}}.\end{aligned}$$

This yields the preconditioner operator:

$$\mathcal{P} : \mathbf{S} \mapsto \tilde{P}_1 \mathbf{S} + \mathbf{S} \tilde{P}_2^\top \quad (31)$$

The whole process is summarized in Algorithm 3.

Algorithm 3: Backward Euler Adaptive-Rank Integrator for the Generalized Sylvester Equation.

// This algorithm solves Eq. (24) for $\mathbf{F}_1 = U_1 S_1 V_1^\top$, where $\mathbf{F}_0 = U_0 S_0 V_0^\top$

Input: Initial condition matrices U_0, V_0, S_0 ;

Operators $P_1, P_2, \{T_{1,i}\}_{i=1}^{\ell_x}, \{T_{2,j}\}_{j=1}^{\ell_y}, \{T_{3,k}\}_{k=1}^{k_x}, \{T_{4,l}\}_{l=1}^{k_y}$;

Tolerances $\epsilon_\kappa, \epsilon, \epsilon_{\text{tol}}$;

Maximum iterations **max_iter**;

Output: Updated bases U_1, V_1 ;

Truncated singular values S_1

- (1) Compute operators $\{A_{1,i}\}_{i=1}^{\ell_x}, \{A_{2,j}\}_{j=1}^{\ell_y}, \{A_{3,k}\}_{k=1}^{k_x}, \{A_{4,l}\}_{l=1}^{k_y}$ according to Eq. (26);
 - (2) **for** $m = 1$ **to** *max_iter* **do**
 - // Step K1.*
 - (3) Truncate to tolerance ϵ_κ ;
 - (4) $U_1 \leftarrow \mathcal{T}_{\epsilon_\kappa} \left(\kappa_m \left(P_1, P_1^{-1}, A_{1,1:\ell_x}^{-1}, A_{3,1:k_x}^{-1}, \Phi_{1:\ell_y}^{1,y}, \Sigma_{1:k_y}^{1,y}, U_0 \right) \right)$;
 - (5) $V_1 \leftarrow \mathcal{T}_{\epsilon_\kappa} \left(\kappa_m \left(P_2, P_2^{-1}, A_{2,1:\ell_y}^{-1}, A_{4,1:k_y}^{-1}, \Phi_{1:\ell_x}^{2,x}, \Sigma_{1:k_x}^{2,x}, V_0 \right) \right)$;
 - // Step K2.*
 - (6) Solve the reduced equation (29) for S_1 using GMRES-ACS (31) to tolerance ϵ_{GMRES} ;
 - // Step K3.*
 - (7) Truncate $\{U_1, S_1, V_1\} \leftarrow \mathcal{T}_\epsilon(\{U_1, S_1, V_1\})$ to tolerance ϵ ;
 - // Step K4.*
 - (8) Compute $\{-, R_U\} = \text{QR} \left([U_1, T_{1,1:\ell_x} U_1, \Phi_{1:\ell_y}^{1,y} U_1, T_{3,1:k_x} U_1, \Sigma_{1:k_y}^{1,y} U_1] \right)$ and
 - (9) $\{-, R_V\} = \text{QR} \left([V_1, \Phi_{1:k_x}^{2,x} V_1, T_{2,1:\ell_y} V_1, \Sigma_{1:k_y}^{2,x} V_1, T_{4,1:k_y} V_1] \right)$;
 - (10) Compute the residual $\|\mathbf{R}\| = \left\| R_U \text{diag} \left(S_1 - \tilde{B}_1, -\Delta t (I_{\mathcal{R}_{\text{ranks}}} \otimes S_1) \right) R_V^\top \right\|$;
 - (11) **if** $\|\mathbf{R}\|/\|\mathbf{F}_0\| \geq \epsilon_{\text{tol}}$ **then**
 - (12) Reject solution and return to augment bases further;
 - (13) **else**
 - (14) Break;
 - (15) Exit loop;
-

The MATLAB implementation of the algorithm is publicly available on GitHub, *Adaptive-rank-ACS*, <https://github.com/helkahza1/Adaptive-rank-ACS>

3.6 Computational Complexity

We now analyze the computational complexity of Algorithm 3 for backward Euler. For conciseness, we consider the same spatial resolution per dimension, i.e., $N = N_1 = N_2$. Starting from an initial condition

$U_0 S_0 V_0^\top$, where $U_0 \in \mathbb{R}^{N \times r_0}$, $V_0 \in \mathbb{R}^{N \times r_0}$, and $S_0 \in \mathbb{R}^{r_0 \times r_0}$, the m -th extended Krylov iteration generates $U_1 \in \mathbb{R}^{N \times r_\kappa}$, $V_1 \in \mathbb{R}^{N \times r_\kappa}$, and $S_1 \in \mathbb{R}^{r_\kappa \times r_\kappa}$, where $r_\kappa = ((2 + \mathcal{R}_{\text{ranks}})m + 1)r_0$. Using SVD-truncated QR, this dimension is then reduced to smaller ranks, r_x and r_y , for the x and y directions, respectively. The matrix S_1 from the m -th Krylov iteration solve, initially of size $r_x \times r_y$, is truncated to rank $r_1 \leq \min(r_x, r_y)$ using Algorithm 2. To simplify the complexity analysis, similar to Section 3.3, let $r = \max(r_x, r_y)$. The computational complexity of each step is then estimated as follows:

Step K1 Constructing the generalized Krylov basis as outlined in lines (4) and (5) of Algorithm 3 requires performing the operations $A_{1,1:r_x}^{-1} U_0$ and $A_{3,1:k_x}^{-1} U_0$, and $A_{2,1:r_y}^{-1} V_0$ and $A_{4,1:k_y}^{-1} V_0$ which necessitates solving the systems $AX = U$ and $AX = V$, where the subscripts have been omitted for simplicity. This is typically achieved through an LU factorization of the operator. With 1D finite differences, A has a tridiagonal structure, which can be efficiently factorized using techniques such as the Thomas algorithm, resulting in a complexity of $\mathcal{O}(N)$ per column of X [28]. The same complexity holds for applying P_1^{-1} and P_2^{-1} . Additionally, applying $P_1 U_0$, $\Phi_{1,3} U_0$, $\Sigma_{1,3} U_0$, $P_2 V_0$, $\Phi_{2,4} V_0$, and $\Sigma_{2,4} V_0$, can be done with $\mathcal{O}(Nr_0)$ computational complexity for sparse diagonal and tridiagonal matrices, leading to a total complexity of $\mathcal{O}(N\mathcal{R}_{\text{ranks}}r_0)$ to form the extended Krylov subspaces.

Regarding truncated orthonormalization in Algorithm 1, using a modified Gram-Schmidt method to compute the reduced QR decomposition of U_1 and V_1 , in line (1), requires a complexity of $\mathcal{O}(Nr_\kappa^2)$. The SVD decomposition of the small-sized upper triangular matrix in line (2) requires complexity $\mathcal{O}(r_\kappa^3)$. The basis update in line (4) requires a complexity of $\mathcal{O}(Nr_\kappa r)$, where $r \leq r_\kappa$. Hence, the complexities of lines (4), (5) in Algorithm 3 scale as $\mathcal{O}(Nr_\kappa^2)$. Generally, we expect $r_\kappa \ll N$ when the solution exhibits a low-rank structure.

Step K2 The application of the operator using matrix-matrix multiplication and summation in the Krylov method (GMRES), as outlined in Section, 3.3, requires a complexity of $\mathcal{O}(r^3)$. Furthermore, applying the preconditioner involves solving a Sylvester equation of size r , which can be achieved using the Bartels-Stewart algorithm [11] with a complexity of $\mathcal{O}(r^3)$. Hence, the S -step has $\mathcal{O}(r^3)$ complexity.

Step K3 The SVD decomposition of \tilde{S} in line (1) of Algorithm 2 is of $\mathcal{O}(r^3)$, also independent of N . Updating the bases in lines (4) and (5) of Algorithm 2 requires $\mathcal{O}(Nrr_1)$, where $r_1 \leq r$ is the post-truncation rank of the new solution as described in Algorithm 2.

Step K4 The QR decomposition to obtain R_U and R_V in lines (9) of Algorithm 3 necessitates a complexity of $\mathcal{O}(N(\mathcal{R}_{\text{ranks}}r_1)^2)$. The residual computation in line (10) is of $\mathcal{O}(r_1^3)$ (i.e., independent of N) due to the matrix multiplications, with an additional $\mathcal{O}(r_1^2)$ for the Frobenius norm.

We note that henceforth r will represent the maximum of r_κ and $\mathcal{R}_{\text{ranks}}r_1$. We conclude that the overall algorithm scales as $\mathcal{O}(Nr^2 + r^3)$, which motivates keeping the overall rank r as low as possible. These scalings will be verified later in this study.

3.7 Extension to High-order Temporal Discretization

The DIRK method features a stage-by-stage backward Euler-like implicit solve, with explicit evaluation of the terms on the right side of the previous Runge-Kutta stages [10]. In Appendix C.1, the mathematical formulation of the DIRK schemes is elaborated leading to the following residual equation for the k -th RK stage,

$$\mathbf{R}_{\mathcal{L}}^{(k)} = \mathbf{F}^{(k)} - a_{kk}\Delta t \mathcal{L}(\mathbf{F}^{(k)}) - \mathbf{B}^{(k)} = \mathbf{0}, \quad \text{with} \quad \mathbf{B}^{(k)} = \mathbf{F}_0 + \Delta t \sum_{\ell=1}^{k-1} a_{k\ell} \mathbf{Y}_\ell, \quad k = 1, 2, \dots, s. \quad (32)$$

Expanding the operator \mathcal{L} in the residual equation above results in the following k -th stage generalized Sylvester equation:

$$\mathbf{F}^{(k)} - a_{k,k}\Delta t \left(T_1 \mathbf{F}^{(k)} \Phi_2^\top + \Phi_1 \mathbf{F}^{(k)} T_2^\top + T_3 \mathbf{F}^{(k)} \Sigma_2^\top + \Sigma_1 \mathbf{F}^{(k)} T_4^\top \right) = \mathbf{B}^{(k)}, \quad k = 1, 2, \dots, s. \quad (33)$$

For the DIRK scheme, we broadly adopt the strategy outlined in [10] with minor modifications to improve efficiency. In particular, we: (i) construct the basis using the time-step of the first stage and retain it for subsequent stages, (ii) evolve the projected system for the S_1 matrix across the DIRK stages, and (iii) truncate and evaluate the residual to determine whether to admit the solution or return to step (i) to further augment the basis. Key modifications vs. [10] include truncating the solution before the residual computation, and only checking the residual at the end of the DIRK step. The reduced matrix is solved similarly to the backward Euler method outlined above, using preconditioned GMRES, where the preconditioner is based on an approximate operator, $\tilde{\mathcal{L}}$. Further details on the discretization of the advection-diffusion equation using the DIRK scheme are provided in Appendix C. Specifically, Appendix C.2 describes the adaptive-rank approach for high-order integration, Appendix C.3 extends the integration to multi-rank coefficients with DIRK schemes and presents a pseudo-algorithm.

4 Numerical Experiments

We demonstrate the computational complexity estimates and the overall efficacy of the proposed algorithm for advection-diffusion equations with several numerical examples. We assume homogeneous Dirichlet boundary conditions for all the tests for simplicity. All simulations were performed using MATLAB. For benchmarking purposes, we compare against full-rank algorithm using the Kronecker formulation inverted with MATLAB's backslash command. Throughout this section, we denote the diffusion Courant number and the advection Courant-Friedrichs-Lewy (CFL) number by λ_D and λ_A , respectively, defined as:

$$\lambda_D = \frac{\Delta t \phi_{\max}}{\Delta x^2}, \quad \lambda_A = \frac{\Delta t \sigma_{\max}}{\Delta x}, \quad (34)$$

where ϕ_{\max} and σ_{\max} are the maximum of the diffusion and advection coefficients, respectively. We set algorithmic tolerances as follows. We first choose the residual tolerance, ϵ_{tol} . One strategy to prevent rapid growth of the extended Krylov subspaces, especially when the matrix equations contain many terms, is to choose the Krylov basis truncation threshold as $\epsilon_\kappa \geq \epsilon_{\text{tol}}$ to truncate basis vectors that are nearly linearly dependent. However, over-truncation may risk removing important information, slowing down convergence. The GMRES tolerance ϵ_{GMRES} is chosen as $\epsilon_{\text{GMRES}} < 10^{-2} \epsilon_{\text{tol}}$ to ensure that the error in the inner loop does not pollute the outer loop. The SVD truncation threshold ϵ are set to $\epsilon < 10^{-2} \epsilon_{\text{tol}}$. Since truncation occurs before residual evaluations, the error introduced by solution truncation must remain below the residual tolerance. Otherwise, the computed solution may meet the residual threshold, but over-truncation could prevent this acceptance.

Example 4.1: Advection-diffusion with a rank-1 advection coefficient and a rank-3 diffusion coefficient

Consider Equation (3) with a rank-1 variable advection coefficient:

$$\begin{aligned} \sigma^x(x, y) &= \sigma_1^1(x) \sigma_1^2(y), \quad \sigma_1^1(x) = 1 - x^2, \quad \sigma_1^2(y) = 2y, \\ \sigma^y(x, y) &= \sigma_2^1(x) \sigma_2^2(y), \quad \sigma_2^1(x) = -2x, \quad \sigma_2^2(y) = 1 - y^2, \end{aligned}$$

and a rank-3 variable diffusion coefficient:

$$\begin{aligned} \phi^x(x, y) &= \phi^y(x, y) = \sum_{i=1}^3 \phi_i^1(x) \phi_i^2(y), \\ \phi_1^1(x) &= \exp\left(-(x - 0.3 \sin(x))^2\right), \quad \phi_1^2(y) = \exp\left(-(y - 0.3 \cos(y))^2\right), \\ \phi_2^1(x) &= \exp\left(-(x - 0.6 \sin(\pi x))^2\right), \quad \phi_2^2(y) = \exp\left(-(y - 0.6 \sin(\pi y))^2\right), \\ \phi_3^1(x) &= \exp\left(-(x - 0.6 \sin(2\pi x))^2\right), \quad \phi_3^2(y) = \exp\left(-(y - 0.6 \sin(2\pi y))^2\right). \end{aligned}$$

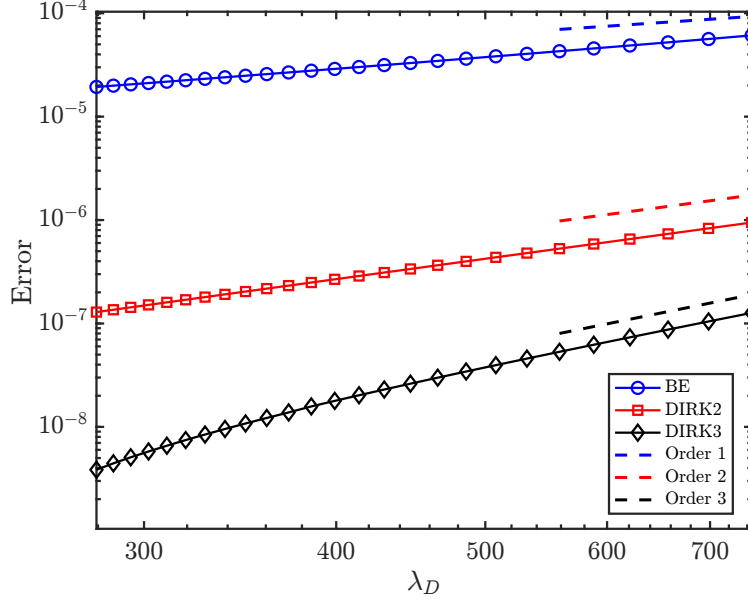


Figure 2: Example 4.1. Temporal convergence study of BE, DIRK2, and DIRK3 schemes.

The initial condition is a rank-2 Gaussian:

$$f(x, y, 0) = 0.5 \exp(-400((x - 0.3)^2 + (y - 0.35)^2)) + 0.8 \exp(-400((x - 0.65)^2 + (y - 0.5)^2)).$$

We use a spatial grid with $N_x = N_y = 300$, and the time-step Δt is set to $\lambda_D \Delta x^2$, with λ_D ranging from 280 to 750. We test our adaptive-rank algorithm using three different integrators: backward Euler (BE), DIRK2, and DIRK3, as detailed in Tables 2 and 3 in the Appendix. The residual tolerance is $\epsilon_{\text{tol}} = 10^{-4}$ for BE, DIRK2, and DIRK3. The basis truncation threshold is $\epsilon_\kappa = 10^{-3}$. The GMRES convergence threshold is $\epsilon_{\text{GMRES}} = 10^{-8}$, and the SVD truncation threshold is $\epsilon = 10^{-8}$.

Figure 2 illustrates the L_1 error norm vs time stepping size characterized by λ_D by showcasing the performance of the adaptive-rank integrator for BE, DIRK2, and DIRK3. The expected temporal error order of convergence for our proposed adaptive-rank integrators, depicted by lines with markers, is observed.

We performed a computational complexity study to demonstrate the proposed algorithm has a linear complexity with respect to N , the number of grid points per dimension. The mesh size $N = N_x = N_y$ varied between 100 and 31000 and the time step was fixed at $\Delta t = 10^{-3}$. This range of mesh sizes is chosen to prevent the $O(r^3)$ contribution of the coefficient matrix GMRES solver from polluting the mesh-resolution scaling.

Figure 3(a) displays N vs. computational time. We observe that the complexity remains linear with respect to N .

Figure 3(b) shows the computational time required for solving the projected generalized Sylvester equation via preconditioned GMRES-ACS vs. rank for a single time step using BE with $N = 10,000$ and $\epsilon_{\text{GMRES}} = 10^{-10}$. To examine the computational scaling corresponding to the expansion of the Krylov basis, we allowed the basis to grow without truncation, recording the simulation time required for the GMRES solve at each basis augmentation iteration. This figure verifies the expected cubic scaling, e.g. $\mathcal{O}(r^3)$. From the above study, we verify that the predominant complexity of our approach is $\mathcal{O}(Nr^2 + r^3)$, effectively reducing the complexity of full rank methods, yet maintain their high-order convergence.

We investigate next the impact of the proposed preconditioner in the S-step by comparing the performance of the GMRES solver with and without the preconditioner. Figure 4 showcases the GMRES residual history as a function of the number of iterations for both preconditioned and unpreconditioned cases for mesh sizes ranging from 200 to 2500, in a single time step with $\Delta t = 0.01$. It is observed that preconditioning significantly accelerates convergence, with the convergence rate independent of the mesh size, which is not the case for unpreconditioned GMRES.

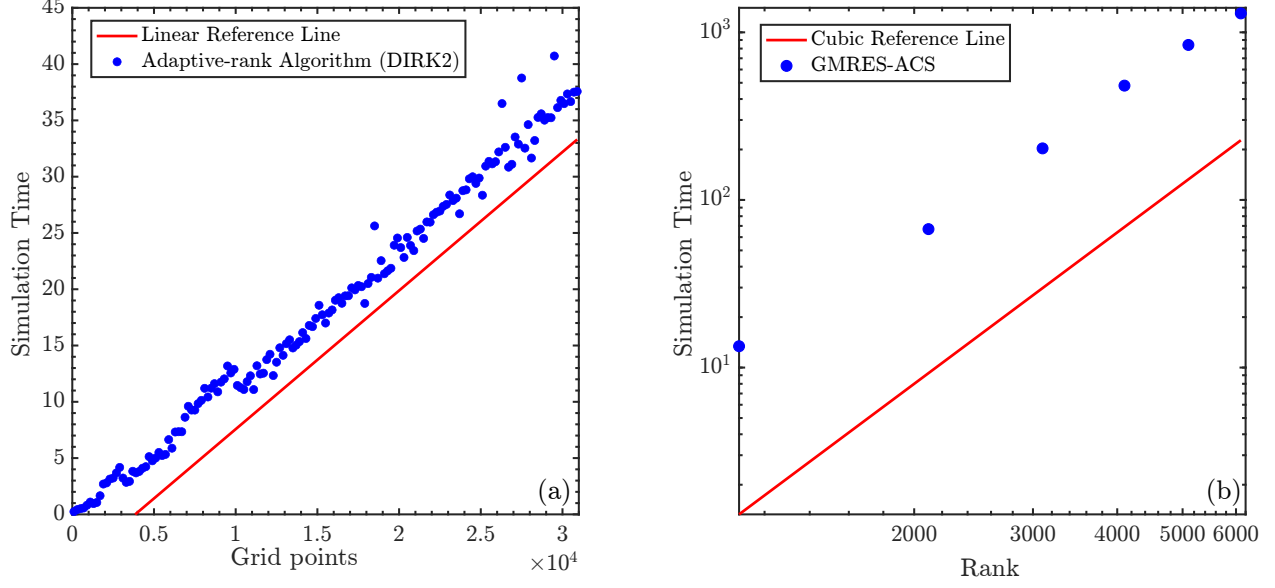


Figure 3: Example 4.1.(a) Computational complexity of DIRK2 adaptive-rank integrator. (b) Log-log plot of GMRES-ACS solver. The execution times were recorded using MATLAB’s `timeit` function.

Example 4.2: Adaptive Rank Evolution with Manufactured Solution

We assess next the performance of the proposed method to capture the rank adaptively using a manufactured solution defined as:

$$\begin{aligned}
 f(x, y, t) = & (\sin(\pi x) \sin(\pi y)) \exp[-0.1\pi(t-2)^2] \\
 & + (\sin(2\pi x) \sin(2\pi y)) \exp[-0.5\pi(t-10)^2] \\
 & + \left(e^{[-100(x-0.3)^2 - 100(y-0.3)^2]} + e^{[-100(x+0.3)^2 - 100(y+0.3)^2]} \right) e^{[-0.5\pi(t-15)^2]}.
 \end{aligned}$$

This solution is initially rank-9 and fluctuates in rank over time, with significant changes at $t = 1, 10$, and 15 . Based on this solution, we analytically compute the source term $S(x, y, t)$. The diffusion coefficients are set as previously described in Example 15.1. We use a spatial grid of $N = 1000$, the BE integrator and simulate until $T_f = 18$. The relative residual tolerance is $\epsilon_{\text{tol}} = 10^{-8}$. The GMRES convergence threshold is set to $\epsilon_{\text{GMRES}} = 10^{-12}$. The singular-value truncation threshold is set to $\epsilon = 10^{-5}$. The Krylov basis truncation threshold is $\epsilon_\kappa = 10^{-5}$. We use a time step $\Delta t = \lambda_D \Delta x^2$ with $\lambda_D = 1300$, or equivalently, $\Delta t = \lambda_A \Delta x$ with $\lambda_A = 17$.

Figure 5(a) tracks the adaptive rank in time with our proposed adaptive rank integrator (in dashed red) vs the full-rank integrator (in solid blue). Agreement is excellent between the two. Figure 5(b) illustrates the evolution of the extended Krylov subspace over time, before and after applying the truncation step in Algorithm 3. Our approach effectively filters out low-relevance basis vectors, maximizing computational efficiency. The extended Krylov basis-augmentation history is shown in the semi-transparent red bars in Figure 5(b) (corresponding to right y-axis). It can be seen that the algorithm performs several (~ 3) iterations of basis augmentation around the $t = 1, 10$, and 15 , to find an appropriate subspace to resolve the rank growth induced by the source term, settling into ~ 1 iteration otherwise. This demonstrates the effectiveness of the Krylov subspace formulation proposed here to find suitable low-rank subspaces as allowed by the dynamics of the solution.

Example 4.3: Swirling Deformation Flow

We consider solving the following advection-diffusion equation:

$$f_t - [(1 - x^2) \cdot 2y \cdot f]_x + [2x \cdot (1 - y^2) \cdot f]_y = \nu \Delta f, \quad x, y \in [-1, 1] \quad (35)$$

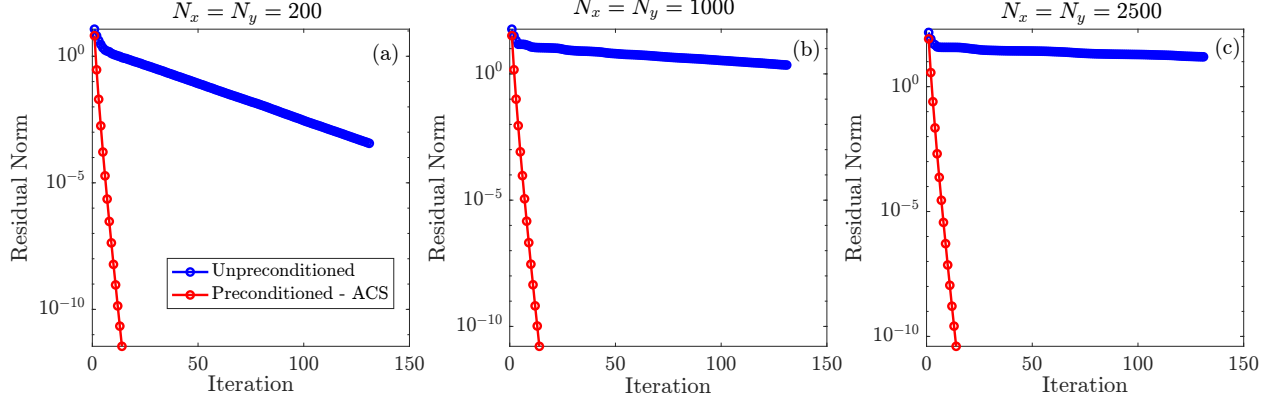


Figure 4: Example 4.1. Semi-log plot of GMRES residuals versus iterations with and without preconditioning. The simulation is conducted for a single time step with $\Delta t = 0.01$, on meshes of size $N_x = N_y = 200$ in (a), $N_x = N_y = 1000$ in (b), and $N_x = N_y = 2500$ in (c).

The initial condition is a bi-Gaussian function given by:

$$f(x, y, 0) = 0.5 \exp\left(-\frac{1}{2\sigma^2} [(x - 0.3)^2 + (y - 0.35)^2]\right) + 0.8 \exp\left(-\frac{1}{2\sigma^2} [(x - 0.65)^2 + (y - 0.5)^2]\right),$$

where $\sigma = 0.15$. We choose the diffusion coefficient $\nu = 10^{-3}$, small enough to weaken the diffusion process. To satisfy the cell-Reynolds number (to preserve monotonicity while keeping the spatial discretization linear; see Appendix B), we set $\Delta x = 9.52 \times 10^{-4}$, resulting in a mesh with $N_x = N_y = 2100$. This test showcases the capability of our proposed low-rank integrator to handle fine meshes, ensuring that the numerical solution adheres to the required monotonicity criteria and avoids unphysical behavior. The residual tolerance is set to $\epsilon_{\text{tol}} = 10^{-5}$, the basis truncation threshold is set to $\epsilon_\kappa = 10^{-3}$, the SVD truncation threshold is set to $\epsilon = 10^{-5}$, and the GMRES acceptance threshold is set to $\epsilon_{\text{GMRES}} = 10^{-10}$.

Figure 6 demonstrates our algorithm's ability to capture the solution rank for this challenging case. The solution rotates according to the prescribed advection coefficients and diffuses slowly over time. As the solution structure becomes more complex due to deformation, the rank increases to accurately represent its physical features. Notably, the algorithm dynamically adjusts the solution rank, which does not exceed $r_1 = 20$, two orders of magnitude smaller than the grid dimension $N = 2100$.

Additionally, we evaluate the algorithm's effectiveness in dynamically capturing the solution rank, even with large time steps. To this end, we use the proposed adaptive-rank algorithm with DIRK3 temporal integration and employ subsequent larger time steps, Δt , corresponding to CFL numbers $\lambda_A = 1$ and $\lambda_A = 15$. All other parameters are kept consistent with the simulation depicted in Figure 6, specifically $\epsilon_\kappa = 10^{-3}$, $\epsilon_{\text{tol}} = 10^{-5}$, $\epsilon = 10^{-5}$, and $\epsilon_{\text{GMRES}} = 10^{-10}$. Figure 7 shows the evolution of the generalized Krylov subspace over time, both before and after truncation, highlighting significant reductions in basis size and thus algorithmic complexity. The figure also demonstrates that the algorithm effectively captures the solution rank evolution even with fairly large (but dynamically relevant) advective CFLs at comparable performance. This demonstrates the algorithm's capability to construct an appropriate Krylov basis, accurately evaluate the effects of the advection and diffusion operators, and dynamically truncate the subspace as needed.

Example 4.4: Constructed Steady-State Solution

In this example, we construct diffusion and advection coefficients that balance each other, resulting in a non-trivial steady-state solution. Specifically, we seek an equilibrium solution satisfying the steady-state condition:

$$0 = \nabla \cdot (\Phi \cdot \nabla f_{\text{eq}} - \Sigma f_{\text{eq}}), \quad (36)$$

a solution of which is:

$$\Sigma = \Phi \cdot \nabla \log(f_{\text{eq}}).$$

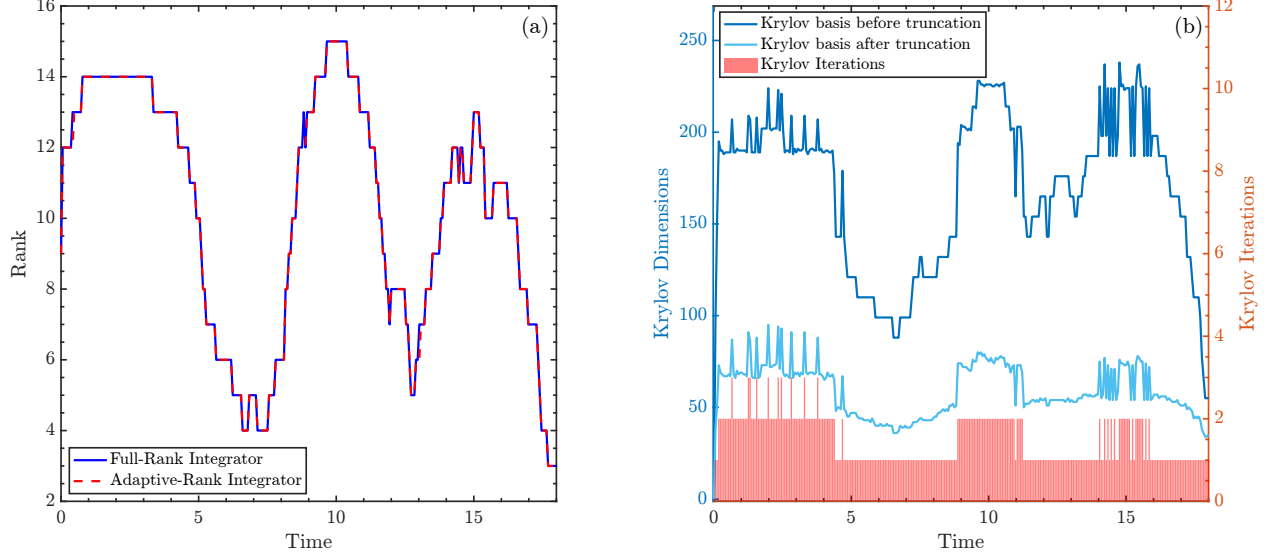


Figure 5: Example 4.2. (a) Rank evolution of the adaptive-rank method using the backward Euler temporal update with a rank-3 manufactured solution. (b) Left axis: evolution of the extended Krylov subspace size over time, both before and after truncation. Right axis: number of Krylov basis iterations required for solution convergence.

This equation defines the steady-state flow from a provided diffusion coefficient and a steady-state solution. We choose the steady-state solution in the domain $0 \leq x, y \leq 1$ to be:

$$f_{\text{eq}}(x, y) = (x(1-x))^2 (y(1-y))^2,$$

which satisfies homogeneous Dirichlet boundary conditions. The diffusion coefficients are defined as:

$$\begin{aligned} \phi^x(x, y) &= \phi^y(x, y) = \phi^1(x)\phi^2(y), \\ \phi^1(x) &= x^2(1-x)^2, \\ \phi^2(y) &= y^2(1-y)^2. \end{aligned}$$

The variable advection coefficients are then given by:

$$\sigma^x(x, y) = \sigma^1(x)\sigma^2(y), \quad D_y(x, y) = \chi^1(x)\chi^2(y),$$

where:

$$\begin{aligned} \sigma^1(x) &= 2x(1-3x+2x^2), & \sigma^2(y) &= y^2(1-y)^2, \\ \chi^1(x) &= x^2(1-x)^2, & \chi^2(y) &= 2y(1-3y+2y^2). \end{aligned}$$

We select the following rank-1 initial condition:

$$f(x, y, 0) = |\sin(2\pi x) \sin(2\pi y)|, \quad 0 \leq x, y \leq 1.$$

Since the solution will converge to a steady state up to a constant, we correct the mass of the initial condition to match that of the steady-state solution. To correct the mass of the solution, we adopt the LoMaC strategy outlined in [14, 13, 12], as implemented in [10]. Figure 8 shows the error of the numerical steady-state solution relative to the prescribed analytical steady state as a function of mesh size. The advection CFL number, λ_A , for a fixed time step $\Delta t = 1000$ ranges from 19,050 to 577,500 as the mesh is refined, indicating the exceptionally large time steps allowed by the algorithm. The results confirm that second-order spatial convergence is achieved and demonstrate that, under these conditions, large time steps can be taken while still accurately reaching the correct steady state with asymptotic convergence.

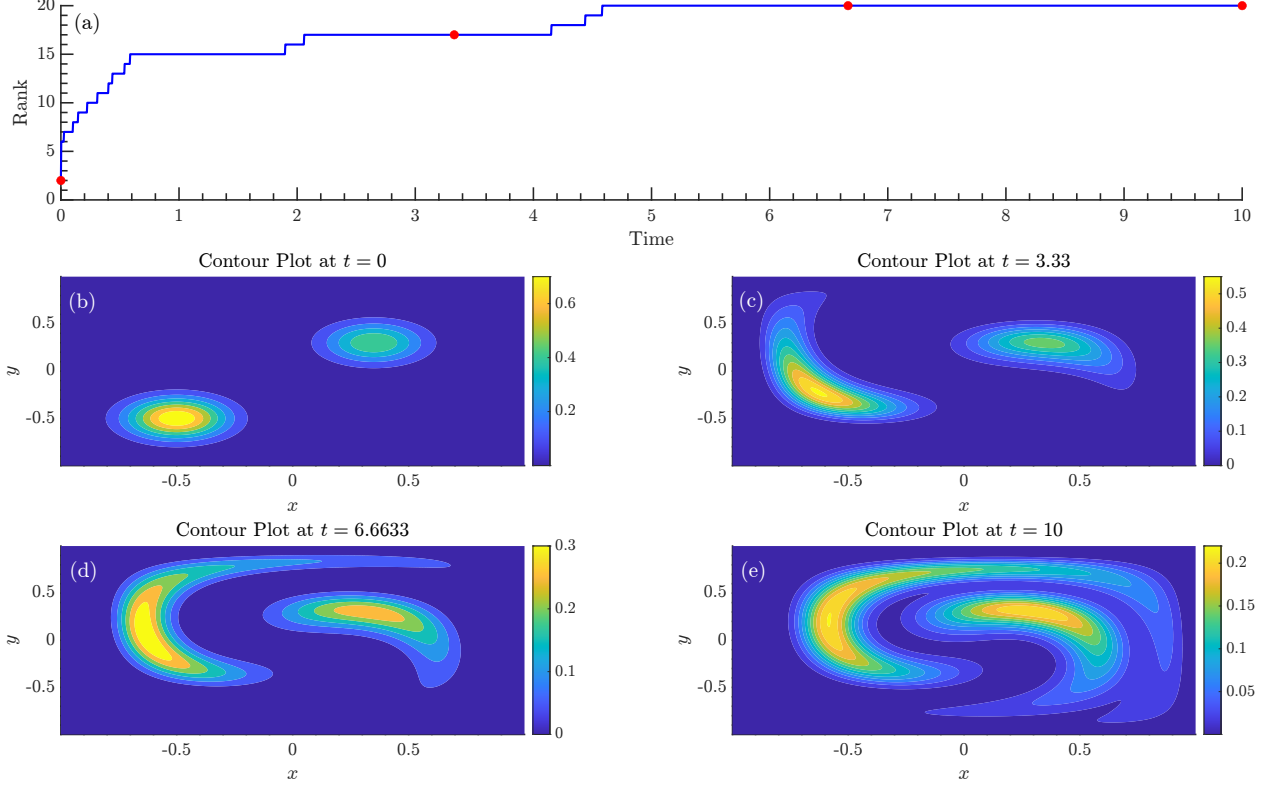


Figure 6: Example 4.3. Swirling deformation problem using DIRK3 with time step corresponding to $\lambda_A = 7$ on a 2100×2100 . (a) Evolution of rank over time. (b)–(e) Solution profiles at $t = 0$, $t = 2.8487$, $t = 5.7088$, and $t = 9.9962$. The final simulation time is $T_f = 10$.

5 Conclusion

We have proposed a computationally efficient adaptive-rank implicit algorithm for solving time-dependent advection-diffusion partial differential equations with variable coefficients. We discretize the PDE using second-order centered finite differences in space and implicitly in time with up to third-order accuracy using DIRK, resulting in a generalized Sylvester matrix equation. Our algorithm is based on several key strategies: constructing dimension-wise basis from extended Krylov subspaces, projecting the original matrix equation onto a reduced system to solve for a coefficient matrix, devising an effective Averaged-Coefficient Sylvester (ACS) preconditioner for the reduced system, and a computationally efficient procedure for the residual evaluation. This combined approach achieves a computational complexity of $\mathcal{O}(Nr^2 + r^3)$, with r being the rank of the solution during Krylov iteration process, effectively mitigating the curse of dimensionality and making it comparable in efficiency to constant-coefficient cases [10]. We have verified our algorithm through a series of numerical experiments. Overall, our adaptive-rank algorithm offers a scalable and efficient solution for time-dependent advection-diffusion type PDEs with variable coefficients. It effectively balances computational cost and accuracy by efficiently constructing and truncating the Krylov basis and dynamically adjusting the solution rank. The ability to handle large meshes and time steps without sacrificing accuracy makes it a promising tool for a wide range of applications. Future research directions include extending the algorithm to higher dimensions and nonlinear PDEs.

Acknowledgements

This work was partially supported by the Multifaceted Mathematics Integrated Capability Centers (MMICCs) program of DOE Office of Applied Scientific Computing Research (ASCR). Los Alamos National Laboratory

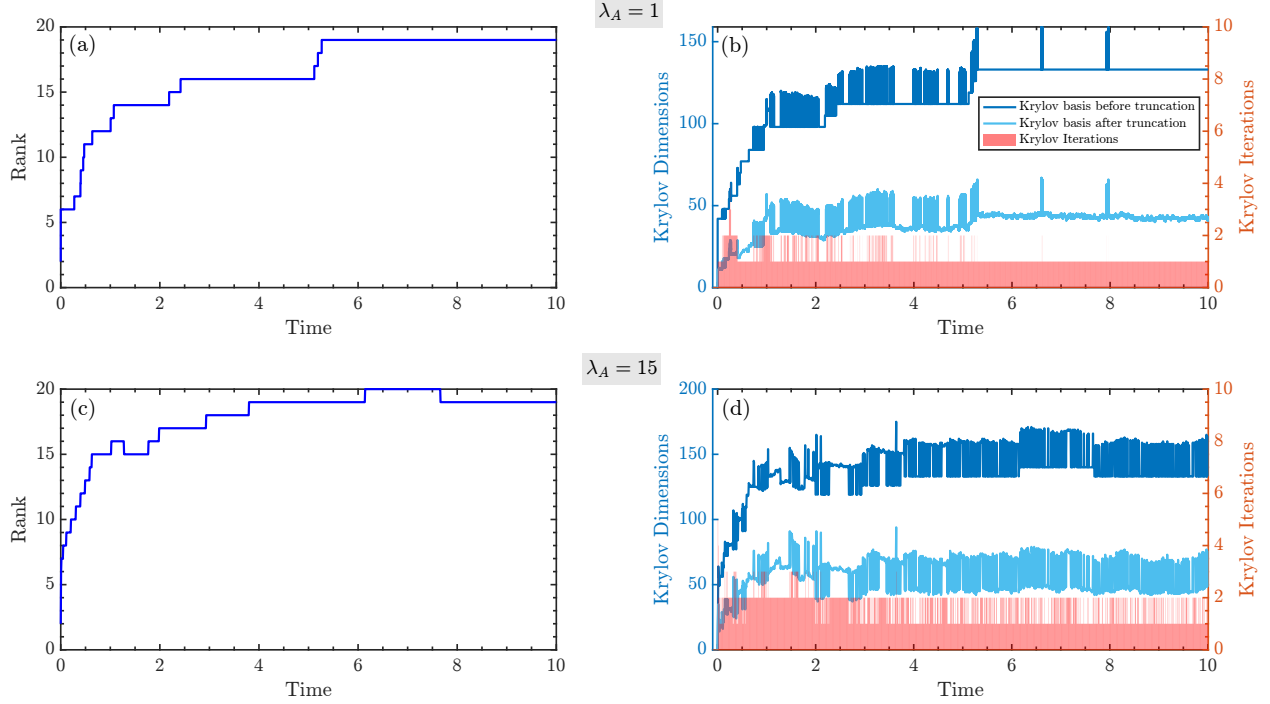


Figure 7: Example 4.3. Evolution of the Extended Krylov subspace over time before and after truncation for different λ_A values using DIRK3: (a) and (b) correspond to $\lambda_A = 1$, while (c) and (d) correspond to $\lambda_A = 15$.

(LANL) is operated by Triad National Security, LLC, for the National Nuclear Security Administration of U.S. Department of Energy (Contract No. 89233218CNA000001). J.Q. and H.E. were supported by NSF grant NSF-DMS-2111253. J.Q. was supported by Air Force Office of Scientific Research FA9550-22-1-0390, Department of Energy DE-SC0023164 and Air Force Office of Scientific Research (AFOSR) FA9550-24-1-0254 via the Multidisciplinary University Research Initiatives (MURI) Program. H.E. was also supported by MMICCs at LANL during the summer of 2024.

A Discretization of the Diffusion Operator

We provide a detailed derivation of the matrix formulation of the discretization of the diffusion operator for the two-dimensional advection-diffusion equation with separable diffusion coefficients. We consider the discretization of the diffusion term in the x -direction, with other directions treated similarly. Consider the diffusion term in the x -direction:

$$\frac{\partial}{\partial x} \left(\phi^x(x, y) \frac{\partial u(x, y)}{\partial x} \right), \quad (37)$$

where the diffusion coefficient is separable:

$$\phi^x(x, y) = \phi^1(x) \phi^2(y). \quad (38)$$

Our goal is to discretize this term using a 3-point stencil on a uniform grid with spacing Δx in the x -direction. Let $u_{i,j} \approx u(x_i, y_j)$, with $i = 0, \dots, N_x - 1$ and $j = 0, \dots, N_y - 1$.

We approximate the spatial derivative using central differences. The discrete approximation at grid point (i, j) is:

$$\left[\frac{\partial}{\partial x} \left(\phi^x \frac{\partial u}{\partial x} \right) \right]_{i,j} \approx \frac{1}{\Delta x} \left[\left(\phi^x \frac{\partial u}{\partial x} \right)_{i+\frac{1}{2},j} - \left(\phi^x \frac{\partial u}{\partial x} \right)_{i-\frac{1}{2},j} \right], \quad (39)$$

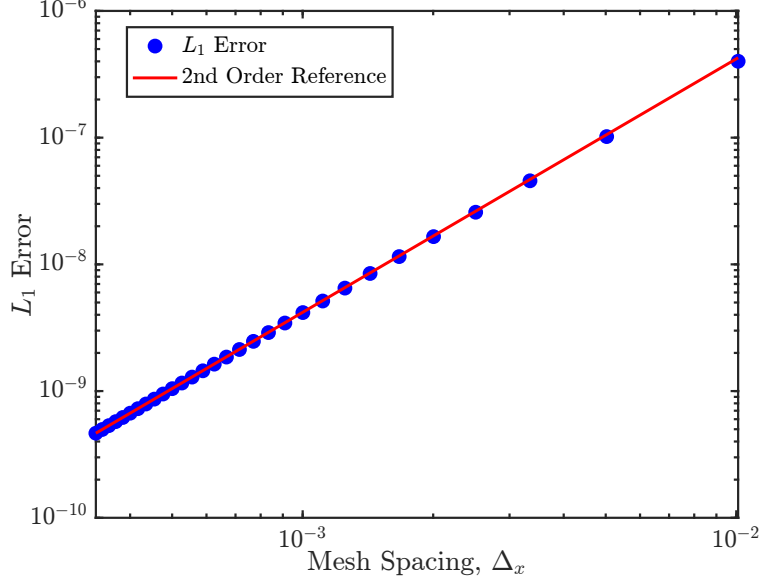


Figure 8: Example 4.4. Log-log plot of error in the numerical steady-state solution compared to the prescribed analytical steady state as a function of mesh size. The advection CFL number, λ_A , ranges from 19,050 to 577,500. The plot demonstrates the retrieval of second-order spatial convergence in the steady state.

where the fluxes at the cell faces are approximated by:

$$\left(\phi^x \frac{\partial u}{\partial x} \right)_{i+\frac{1}{2},j} \approx \phi_{i+\frac{1}{2},j}^x \cdot \frac{u_{i+1,j} - u_{i,j}}{\Delta x}, \quad (40)$$

$$\left(\phi^x \frac{\partial u}{\partial x} \right)_{i-\frac{1}{2},j} \approx \phi_{i-\frac{1}{2},j}^x \cdot \frac{u_{i,j} - u_{i-1,j}}{\Delta x}. \quad (41)$$

Here $\phi_{i+\frac{1}{2},j}^x = \phi_{i+\frac{1}{2}}^1 \phi_j^2 = \phi^1(x_{i+\frac{1}{2}}) \phi^2(y_j)$. Substituting back into Eq. (39), we obtain:

$$\left[\frac{\partial}{\partial x} \left(\phi^x \frac{\partial u}{\partial x} \right) \right]_{i,j} \approx \frac{1}{\Delta x^2} \left[\phi_{i+\frac{1}{2}}^1 (u_{i+1,j} - u_{i,j}) - \phi_{i-\frac{1}{2}}^1 (u_{i,j} - u_{i-1,j}) \right] \phi_j^2. \quad (42)$$

To express the discretization in matrix form, we define:

- \mathbf{F} : matrix of solution values, $[\mathbf{F}]_{i,j} = f_{i,j}$.
- Φ_+^1 : diagonal matrix with elements $[\Phi_+^1]_{i,i} = \phi_{i+\frac{1}{2}}^1$.
- Φ_-^1 : diagonal matrix with elements $[\Phi_-^1]_{i,i} = \phi_{i-\frac{1}{2}}^1$.
- Φ_2 : diagonal matrix with elements $[\Phi_2]_{j,j} = \phi_j^2$.

We also define the forward and backward difference matrices in the x -direction for the interior nodes $i = 1, \dots, N_x - 2$, where $i = 0$ and $i = N_x - 1$ correspond to zero Dirichlet boundary conditions and rest at the

boundary:

$$D_+ = \frac{1}{\Delta x} \begin{pmatrix} -1 & 1 & 0 & \cdots & 0 \\ 0 & -1 & 1 & \cdots & 0 \\ \vdots & \ddots & \ddots & \ddots & \vdots \\ 0 & \cdots & 0 & -1 & 1 \\ 0 & \cdots & 0 & 0 & -1 \end{pmatrix}, \quad (43)$$

$$D_- = \frac{1}{\Delta x} \begin{pmatrix} 1 & 0 & 0 & \cdots & 0 \\ -1 & 1 & 0 & \cdots & 0 \\ 0 & -1 & 1 & \cdots & 0 \\ \vdots & \ddots & \ddots & \ddots & \vdots \\ 0 & \cdots & 0 & -1 & 1 \end{pmatrix}. \quad (44)$$

Using these definitions, the discrete diffusion term in Eq. (42) can be represented in the matrix form as:

$$(\Phi_+^1 D_+ - \Phi_-^1 D_-) \mathbf{F} \Phi_2^\top. \quad (45)$$

We note that the operator multiplying \mathbf{F} from the left is analogous to D_{xx}^Φ in Equation (6). The discretization in the y -direction follows the same strategy.

B Discretization of the Advection Operator

We provide a detailed derivation of the matrix formulation of the discretization of the advection operator for the two-dimensional advection-diffusion equation with variable, separable advection coefficients. As before, we focus on the discretization of the advection term in the x -direction:

$$\frac{\partial}{\partial x} (\sigma^x(x, y) u(x, y)), \quad (46)$$

where the advection coefficient is separable:

$$\sigma^x(x, y) = \sigma^1(x) \sigma^2(y). \quad (47)$$

Our goal is to discretize this term on a uniform grid with spacing Δx in the x -direction and Δy in the y -direction. Let $u_{i,j} \approx u(x_i, y_j)$. To preserve linearity of our discretization without introducing too much numerical dissipation, we employ a central difference scheme to approximate the spatial derivative. This discretization is not monotonicity-preserving unless the so-called cell Reynolds number condition is satisfied:

$$\text{Re}_c = \frac{\sigma_{\max} \Delta x}{\phi_{\max}} < 2, \quad (48)$$

where σ_{\max} is the maximum magnitude of the advection velocity, and ϕ_{\max} is the maximum diffusion coefficient. This condition is practical in our formulation due to the very favorable scaling of our low-rank representation with mesh size and rank.

The discrete approximation at grid point (i, j) is:

$$\left[\frac{\partial}{\partial x} (\sigma^x(x, y) u(x, y)) \right]_{i,j} \approx \frac{1}{\Delta x} \left[(\sigma^x u)_{i+\frac{1}{2},j} - (\sigma^x u)_{i-\frac{1}{2},j} \right], \quad (49)$$

where the fluxes at the cell faces are approximated by:

$$(\sigma^x u)_{i+\frac{1}{2},j} \approx \sigma_{i+\frac{1}{2}}^1 \sigma_j^2 \cdot \frac{u_{i+1,j} + u_{i,j}}{2}, \quad (50)$$

$$(\sigma^x u)_{i-\frac{1}{2},j} \approx \sigma_{i-\frac{1}{2}}^1 \sigma_j^2 \cdot \frac{u_{i,j} + u_{i-1,j}}{2}. \quad (51)$$

Here, $\sigma_{i+\frac{1}{2}}^1 = \sigma^1(x_{i+\frac{1}{2}})$ is the advection coefficient evaluated at the midpoint between x_i and x_{i+1} , and similarly for $\sigma_{i-\frac{1}{2}}^1$. Substituting back into the discrete approximation, we have:

$$\left[\frac{\partial}{\partial x} (\sigma^x(x, y) u(x, y)) \right]_{i,j} \approx \frac{1}{\Delta x} \left[\sigma_{i+\frac{1}{2}}^1 \sigma_j^2 \cdot \frac{u_{i+1,j} + u_{i,j}}{2} - \sigma_{i-\frac{1}{2}}^1 \sigma_j^2 \cdot \frac{u_{i,j} + u_{i-1,j}}{2} \right] \quad (52)$$

$$= \frac{1}{2\Delta x} \left[\sigma_{i+\frac{1}{2}}^1 (u_{i+1,j} + u_{i,j}) - \sigma_{i-\frac{1}{2}}^1 (u_{i,j} + u_{i-1,j}) \right] \sigma_j^2. \quad (53)$$

To express the discretization in matrix form, we define:

- \mathbf{F} : matrix of solution values, $[\mathbf{F}]_{i,j} = f_{i,j}$.
- Σ_+^1 and Σ_-^1 : diagonal matrices with elements $[\Sigma_+^1]_{i,i} = \sigma_{i+\frac{1}{2}}^1$ and $[\Sigma_-^1]_{i,i} = \sigma_{i-\frac{1}{2}}^1$.
- Σ_2 : diagonal matrix with elements $[\Sigma_2]_{j,j} = \sigma_j^2$.

We also define the difference matrices in the x -direction:

$$S_+ = \frac{1}{2} \begin{pmatrix} 1 & 1 & 0 & \cdots & 0 \\ 0 & 1 & 1 & \cdots & 0 \\ \vdots & \ddots & \ddots & \ddots & \vdots \\ 0 & \cdots & 0 & 1 & 1 \\ 0 & \cdots & 0 & 0 & 1 \end{pmatrix}, \quad (54)$$

$$S_- = \frac{1}{2} \begin{pmatrix} 1 & 0 & 0 & \cdots & 0 \\ 1 & 1 & 0 & \cdots & 0 \\ 0 & 1 & 1 & \cdots & 0 \\ \vdots & \ddots & \ddots & \ddots & \vdots \\ 0 & \cdots & 0 & 1 & 1 \end{pmatrix}. \quad (55)$$

Using these definitions, the discrete advection term in the x -direction can be represented as:

$$\frac{1}{\Delta x} (\Sigma_+^1 S_+ - \Sigma_-^1 S_-) \mathbf{F} \Sigma_2^\top. \quad (56)$$

We note that the operator multiplying \mathbf{F} from the left is analogous to D_x^Σ in Equation (6). The discretization in the y -direction follows the same strategy.

C High-order Temporal Discretization

We extend the backward Euler implicit integrator to higher-order DIRK time discretizations for the advection-diffusion operator, as compactly written in (8).

C.1 DIRK Scheme

DIRK methods are characterized by the Butcher tableau, as shown in Table 1. We focus on stiffly accurate DIRK methods, where the coefficients satisfy $b_i = a_{si}$ for $i = 1, \dots, s$, ensuring that the final solution update corresponds to the solution at the last DIRK stage. For instance the Butcher tables for DIRK2 and DIRK3 are presented in Tables 2 and 3, respectively.

Similarly to the backward Euler case, the matrix-based discretization of the advection-diffusion equation using the operator \mathcal{L} defined in (8) results in a generalized Sylvester equation that must be solved at each DIRK stage. The corresponding DIRK scheme for the matrix differential equation (8) from $t^{(0)}$ to $t^{(1)}$ is

Table 1: Butcher tableau for an s -stage DIRK scheme. Here, s represents the number of stages in DIRK, c_i represents the intermediate stage, a_{ij} is a lower-triangular matrix with coefficients used to approximate the solution at each stage, and b_j are the quadrature weights used to update the solution in the final step.

c_1	a_{11}	0	\dots	0
c_2	a_{21}	a_{22}	\dots	0
\vdots	\vdots	\vdots	\ddots	\vdots
c_s	a_{s1}	a_{s2}	\dots	a_{ss}
	b_1	b_2	\dots	b_s

γ	γ	0
1	$1 - \gamma$	γ
	$1 - \gamma$	γ

Table 2: DIRK2 Butcher table with $\gamma = 1 - \frac{\sqrt{2}}{2}$.

x	x	0	0
$\frac{1+x}{2}$	$\frac{1-x}{2}$	x	0
1	$-\frac{3x^2}{2} + 4x - \frac{1}{4}$	$-\frac{3x^2}{2} - 5x + \frac{5}{4}$	x
	$-\frac{3x^2}{2} + 4x - \frac{1}{4}$	$-\frac{3x^2}{2} - 5x + \frac{5}{4}$	x

Table 3: DIRK3 Butcher table with $x = 0.4358665215$.

written as:

$$\mathbf{F}^{(k)} = \mathbf{F}_0 + \Delta t \sum_{\ell=1}^k a_{k\ell} \mathbf{Y}_\ell, \quad k = 1, 2, \dots, s, \quad (57a)$$

$$\mathbf{Y}_k = \mathcal{L}(\mathbf{F}^{(k)}; t^{(k)}), \quad t^{(k)} = t^0 + c_k \Delta t, \quad k = 1, 2, \dots, s, \quad (57b)$$

$$\mathbf{F}_1 = \mathbf{F}^{(s)} = \mathbf{F}_0 + \Delta t \sum_{k=1}^s b_k \mathbf{Y}_k. \quad (57c)$$

More compactly, within each stage k of the DIRK scheme, one must minimize the residual equation (32) given by:

$$\mathbf{R}_{\mathcal{L}}^{(k)} = \mathbf{F}^{(k)} - a_{kk} \Delta t \mathcal{L}(\mathbf{F}^{(k)}) - \mathbf{B}^{(k)} = \mathbf{0}, \quad \text{with} \quad \mathbf{B}^{(k)} = \mathbf{F}_0 + \Delta t \sum_{\ell=1}^{k-1} a_{k\ell} \mathbf{Y}_\ell, \quad k = 1, 2, \dots, s.$$

As shown in Equation (33), the residual equations lead to a generalized Sylvester equation to be solved at each stage.

C.2 Adaptive-Rank Strategy for High-Order Temporal Discretization via DIRK

The high-order DIRK method features a stage-by-stage generalized-Sylvester-equation solve. Our strategy follows closely that of the backward Euler adaptive-rank treatment in that we construct an approximation to the operator, $\tilde{\mathcal{L}}$, which is used for both the basis construction of U_1 and V_1 and the preconditioning of the reduced system to solve S_1 .

At each stage k of the DIRK scheme, the corresponding DIRK formulation for the matrix differential equation from $t^{(0)}$ to $t^{(1)}$ requires solving a Sylvester equation for the approximated operator $\tilde{\mathcal{L}}$ by minimizing the k th-stage residual:

$$\mathbf{R}_{\tilde{\mathcal{L}}}^{(k)} = \mathbf{F}_1 - a_{kk} \Delta t \tilde{\mathcal{L}}(\mathbf{F}_1) - \mathbf{F}_0 - \mathbf{B}^{(k)} = \mathbf{0}, \quad \text{with} \quad \mathbf{B}^{(k)} = \mathbf{F}_0 + \Delta t \sum_{\ell=1}^{k-1} a_{k\ell} \mathbf{Y}_\ell.$$

Expanding this residual using $\tilde{\mathcal{L}}$, defined in (14), leads to the k th-stage Sylvester equation:

$$\underbrace{\left[\underbrace{\left(\frac{1}{4}I - a_{kk}\Delta t \alpha_2 T_1 \right)}_{A_1} + \underbrace{\left(\frac{1}{4}I - a_{kk}\Delta t \gamma_2 T_3 \right)}_{A_3} \right] \mathbf{F}^{(k)} + \mathbf{F}^{(k)}}_{P_1} + \underbrace{\left[\underbrace{\left(\frac{1}{4}I - a_{kk}\Delta t \alpha_1 T_2 \right)^\top}_{A_2^\top} + \underbrace{\left(\frac{1}{4}I - a_{kk}\Delta t \gamma_1 T_4 \right)^\top}_{A_4^\top} \right]}_{P_2^\top} = \mathbf{B}^{(k)}. \quad (58)$$

Note that the operators $A_{1:4}$ are fixed throughout the stages since the DIRK method uses constant diagonal Butcher tableau coefficients.

We follow the strategy discussed in [10] to perform high-order integration. The key idea is to consider the basis fixed across DIRK stages, and only evolve the matrix of coefficients S_1 through the stages. The proposed procedure is as follows:

Step 1. Prediction of Krylov basis functions: construct a set of orthonormal bases U_1 and V_1 from the Krylov-based low-rank implicit solver at the first DIRK stage, i.e. backward Euler with time stepping size $c_1\Delta t$.

Step 2. For $k = 1 : s$ (per DIRK stage)

(a) Solve reduced Sylvester equation for $S^{(k)}$ using preconditioned GMRES,

$$\mathbf{S}^{(k)} - \Delta t \left(\tilde{T}_1 \mathbf{S}^{(k)} \tilde{\Phi}_2^\top + \tilde{\Phi}_1 \mathbf{S}^{(k)} \tilde{T}_2^\top + \tilde{T}_3 \mathbf{S}^{(k)} \tilde{\Sigma}_2^\top + \tilde{\Sigma}_1 \mathbf{S}^{(k)} \tilde{T}_4^\top \right) = \tilde{\mathbf{B}}^{(k)}, \quad (59)$$

with

$$\tilde{\mathbf{B}}^{(k)} = U_1^\top \mathbf{F}_0 V_1 + \Delta t \sum_{\ell=1}^{k-1} a_{k\ell} \tilde{Y}_\ell,$$

Here $\tilde{Y}_\ell = U_1^\top Y_\ell V_1 \in \mathbb{R}^{r_x \times r_y}$. The preconditioner used is given by

$$\mathbf{S} \mapsto \tilde{P}_1 \mathbf{S} + \mathbf{S} \tilde{P}_2, \quad (60)$$

where $\tilde{P}_1 = U_1^\top P_1 U_1$ and $\tilde{P}_2 = V_1^\top P_1 V_1$, and is valid for all stages since the basis constructed is fixed through the DIRK stages by assumption. Solve for $S^{(k)}$ and obtain the intermediate RK solutions as $U_1 S^{(k)} V_1^\top$. To further improve computational efficiency, from (59), we have,

$$\tilde{Y}_\ell = \frac{1}{a_{\ell\ell}\Delta t} \left(S^{(\ell)} - \tilde{B}^{(\ell)} \right),$$

leading to an efficient computation of $\tilde{B}^{(k)}$:

$$\tilde{B}^{(k)} = \tilde{B}_1 + \Delta t \sum_{\ell=1}^{k-1} \frac{a_{k\ell}}{a_{\ell\ell}} \left(S^{(\ell)} - \tilde{B}^{(\ell)} \right), \quad (61)$$

with \tilde{B}_1 defined in (19). This avoids the need of evaluating the full size $B^{(k)}$ in (32).

Step 3. Perform truncation of evolved solution, i.e. $\{U_1, S_1, V_1^\top\} \leftarrow \mathcal{T}_\epsilon(\{U_1, S_1, V_1^\top\})$, with $S_1 := S_1^{(s)}$.

Step 4. Efficiently evaluate the residual norm,

$$\left\| \mathbf{R}_{\mathcal{L}}^{(s)} \right\| = \left\| R_U \text{diag} \left(S_1 - \tilde{B}_1^{(s)}, -a_{ss}\Delta t (I_{\mathcal{R}_{\text{ranks}}} \otimes S_1) \right) R_V^\top \right\|,$$

where R_U and R_V are upper triangular matrices from a reduced QR decomposition as described in (23), which can be done once for all DIRK stages.

1. Compare the computed residual norm $\|\mathbf{R}_{\mathcal{L}}^{(s)}\|$ with the given error tolerance ϵ_{tol} . If the tolerance is met, then admit the solution with $\mathbf{F}_1 = U_1 S_1 V_1^\top$; otherwise, we go back to Step 1 to further augment Krylov subspaces.

C.3 DIRK Generalization to Multi-Rank Advection-Diffusion Coefficients

We now extend the formulation to the multi-rank case, as described in (4). Using a DIRK method for temporal discretization, the k -th stage generalized Sylvester equation becomes:

$$\mathbf{F}^{(k)} - a_{kk} \Delta t \underbrace{\left(\sum_{i=1}^{\ell_x} T_{1,i} \mathbf{F}^{(k)} \Phi_i^{2,x\top} + \sum_{j=1}^{\ell_y} \Phi_j^{1,y} \mathbf{F}^{(k)} T_{2,j}^\top + \sum_{k=1}^{k_x} T_{3,k} \mathbf{F}^{(k)} \Sigma_k^{2,x\top} + \sum_{l=1}^{k_y} \Sigma_l^{1,y} \mathbf{F}^{(k)} T_{4,l}^\top \right)}_{\mathcal{L}(\mathbf{F}^{(k)})} = \mathbf{B}^{(k)}, \quad k = 1, 2, \dots, s \quad (62)$$

where $\mathbf{B}^{(k)}$ is as defined in (32). The terms $T_{1:4,i}$ represent compositions of difference operators with diffusion and advection coefficients, similar to (7). Left subscripts 1 and 2 correspond to diffusion, while 3 and 4 correspond to advection in the x and y directions, respectively. The right subscript denotes the rank of the respective diffusion and advection coefficients. This equation generalizes (10), which is recovered for $\ell_x = \ell_y = k_x = k_y = 1$ and equal diffusion and advection coefficients in both the x and y directions. It also generalizes the backward Euler special case with a single stage and $a_{1,1} = 1$, yielding $\mathbf{B}^{(1)} = \mathbf{F}_0$, consistently with (10).

Using approximations in (25), we arrive at the k th stage approximated Sylvester equation:

$$\underbrace{P_1 \mathbf{F}^{(k)} + \mathbf{F}^{(k)} P_2^\top}_{\tilde{\mathcal{L}}(\mathbf{F}^{(k)})} = \mathbf{B}^{(k)}, \quad (63)$$

where

$$P_1 = \sum_{i=1}^{\ell_x} A_{1,i} + \sum_{k=1}^{k_x} A_{3,k} = \sum_{i=1}^{\ell_x} \left(\frac{1}{\mathcal{R}_{\text{ranks}}} I_{N_1} - a_{kk} \Delta t \alpha_{x,i} T_{1,i} \right) + \sum_{k=1}^{k_x} \left(\frac{1}{\mathcal{R}_{\text{ranks}}} I_{N_1} - a_{kk} \Delta t \gamma_{x,k} T_{3,k} \right),$$

$$P_2 = \sum_{j=1}^{\ell_y} A_{2,j} + \sum_{l=1}^{k_y} A_{4,l} = \sum_{j=1}^{\ell_y} \left(\frac{1}{\mathcal{R}_{\text{ranks}}} I_{N_2} - a_{kk} \Delta t \alpha_{y,j} T_{2,j} \right) + \sum_{l=1}^{k_y} \left(\frac{1}{\mathcal{R}_{\text{ranks}}} I_{N_2} - a_{kk} \Delta t \gamma_{y,l} T_{4,l} \right).$$

In order to obtain a reduced equation for the k th stage matrix of coefficients $\mathbf{S}^{(k)}$, we perform a Galerkin projection $U^\top \mathbf{R}_{\mathcal{L}} V = 0$ to obtain :

$$\mathbf{S}^{(k)} - a_{kk} \Delta t \left(\sum_{i=1}^{\ell_x} \tilde{T}_{1,i} \mathbf{S}^{(k)} \tilde{\Phi}_i^{2,x\top} + \sum_{j=1}^{\ell_y} \tilde{\Phi}_j^{1,y} \mathbf{S}^{(k)} \tilde{T}_{2,j}^\top + \sum_{k=1}^{k_x} \tilde{T}_{3,k} \mathbf{S}^{(k)} \tilde{\Sigma}_k^{2,x\top} + \sum_{l=1}^{k_y} \tilde{\Sigma}_l^{1,y} \mathbf{S}^{(k)} \tilde{T}_{4,l}^\top \right) = \tilde{\mathbf{B}}^{(k)} \quad (64)$$

where the projected operators are analogous to those defined in the rank-one case.

Afterwards, as before, we solve (64) for the $\mathbf{S}^{(k)}$ matrix using preconditioned GMRES. The preconditioner is constructed by a Galerkin projection $U^\top \mathbf{R}_{\tilde{\mathcal{L}}} V = 0$, to find the projected Sylvester equation:

$$\underbrace{\left[\sum_{i=1}^{\ell_x} \tilde{A}_{1,i} + \sum_{k=1}^{k_x} \tilde{A}_{3,k} \right]}_{\tilde{P}_1} \mathbf{S}^{(k)} + \mathbf{S}^{(k)} \underbrace{\left[\sum_{j=1}^{\ell_y} \tilde{A}_{2,j} + \sum_{l=1}^{k_y} \tilde{A}_{4,l} \right]}_{\tilde{P}_2^\top} = \tilde{\mathbf{B}}^{(k)} \quad (65)$$

Using the operators \tilde{P}_1 and \tilde{P}_2 , we define the preconditioner mapping:

$$\mathbf{S} \mapsto \tilde{P}_1 \mathbf{S} + \mathbf{S} \tilde{P}_2^\top, \quad (66)$$

Algorithm 4 solves the variable advection diffusion equation using DIRK methods.

Algorithm 4: s-Stages Adaptive-Rank DIRK Integrator for the Generalized Sylvester Equation.

Input: Initial condition matrices U_0, V_0, S_0 ;
Operators $P_1, P_2, \{T_{1,i}\}_{i=1}^{\ell_x}, \{T_{2,j}\}_{j=1}^{\ell_y}, \{T_{3,k}\}_{k=1}^{k_x}, \{T_{4,l}\}_{l=1}^{k_y}$;
Butcher table $\{a_{ij}\}$;
Time step size Δt ;
Tolerances $\epsilon_\kappa, \epsilon, \epsilon_{\text{tol}}$;
Maximum iterations **max_iter**;
Output: Updated bases U_1, V_1 ;
Truncated singular values S_1 ;

- (1) Compute operators $\{A_{1,i}\}_{i=1}^{\ell_x}, \{A_{2,j}\}_{j=1}^{\ell_y}, \{A_{3,k}\}_{k=1}^{k_x}, \{A_{4,l}\}_{l=1}^{k_y}$ according to Eq. (63);
 - (2) **for** $m = 1$ **to** max_iter **do**
 - // Step 1.
 - (3) Truncate to tolerance ϵ_κ ;
 - (4) $U_1 \leftarrow \mathcal{T}_{\epsilon_\kappa} \left(\kappa_m \left(P_1, P_1^{-1}, A_{1,1:\ell_x}^{-1}, A_{3,1:k_x}^{-1}, \Phi_{1:\ell_y}^{1,y}, \Sigma_{1:k_y}^{1,y}, U_0 \right) \right)$;
 - (5) $V_1 \leftarrow \mathcal{T}_{\epsilon_\kappa} \left(\kappa_m \left(P_2, P_2^{-1}, A_{2,1:\ell_y}^{-1}, A_{4,1:k_y}^{-1}, \Phi_{1:\ell_x}^{2,x}, \Sigma_{1:k_x}^{2,x}, V_0 \right) \right)$;
 - (6) Compute $\tilde{B}^{(1)} = (U_1^\top U_0) S_0 (V_1^\top V_0)^\top$;
 - // Step 2.
 - (7) **for** $k = 1$ **to** s **do**
 - (8) Compute $\tilde{B}^{(k)} = \tilde{B}^{(1)} + \Delta t \sum_{\ell=1}^{k-1} \frac{a_{k\ell}}{a_{\ell\ell}} \left(S^{(\ell)} - \tilde{B}^{(\ell)} \right)$;
 - (9) Solve the reduced equation (65) for $S^{(k)}$ using GMRES with ACS preconditioner (66) to tolerance ϵ_{GMRES} ;
 - (10) Compute and store $\frac{1}{a_{kk}} \left(S^{(k)} - \tilde{B}^{(k)} \right)$ and proceed to the next stage;
 - (11) Truncate $\{U_1, S_1, V_1\} \leftarrow \mathcal{T}_\epsilon(\{U_1, S^{(s)}, V_1\})$ to tolerance ϵ ;
 - // Step 3.
 - (12) Compute $\{-, R_U\} = \text{QR} \left([U_1, T_{1,1:\ell_x} U_1, \Phi_{1:\ell_y}^{1,y} U_1, T_{3,1:k_x} U_1, \Sigma_{1:k_y}^{1,y} U_1] \right)$ and
 - (13) $\{-, R_V\} = \text{QR} \left([V_1, \Phi_{1:\ell_x}^{2,x} V_1, T_{2,1:\ell_y} V_1, \Sigma_{1:k_x}^{2,x} V_1, T_{4,1:k_y} V_1] \right)$;
 - // Step 4.
 - (14) Compute the residual $\|\mathbf{R}\| = \left\| R_U \text{diag} \left(S_1 - \tilde{B}^{(s)}, -a_{ss} \Delta t (I_{\mathcal{R}_{\text{ranks}}} \otimes S_1) \right) R_V^\top \right\|$;
 - (15) **if** $\|\mathbf{R}\| / \|\mathbf{F}_0\| \geq \epsilon_{\text{tol}}$ **then**
 - (16) Return to Step 1 to augment bases further;
 - (17) **else**
 - (18) Break;
 - (19) Exit loop;
-

The MATLAB implementation of the algorithm is publicly available on GitHub, *Adaptive-rank-ACS*, <https://github.com/helkaha1/Adaptive-rank-ACS>

References

- [1] P. Benner and T. Breiten. Low rank methods for a class of generalized lyapunov equations and related issues. *Numerische Mathematik*, 124(3):441–470, 2013.
- [2] T. Breiten, V. Simoncini, M. Stoll, et al. *Fast iterative solvers for fractional differential equations*. Max Planck Institute for Dynamics of Complex Technical Systems, 2014.
- [3] J. R. Bunch. Complexity of sparse elimination. In J. F. Traub, editor, *Complexity of Sequential and Parallel Numerical Algorithms*, pages 197–220. Academic.

- [4] S. L. Campbell, I. C. Ipsen, C. T. Kelley, and C. D. Meyer. Gmres and the minimal polynomial. *BIT Numerical Mathematics*, 36(4):664–675, 1996.
- [5] G. Ceruti and C. Lubich. An unconventional robust integrator for dynamical low-rank approximation. *BIT Numerical Mathematics*, 62(1):23–44, 2022.
- [6] J. W. Daniel. The conjugate gradient method for linear and nonlinear operator equations. *SIAM Journal on Numerical Analysis*, 4(1):10–26, 1967.
- [7] A. Dektor, A. Rodgers, and D. Venturi. Rank-adaptive tensor methods for high-dimensional nonlinear pdes. *Journal of Scientific Computing*, 88(2):36, 2021.
- [8] A. Dektor and D. Venturi. Dynamic tensor approximation of high-dimensional nonlinear pdes. *Journal of Computational Physics*, 437:110295, 2021.
- [9] V. Druskin and L. Knizhnerman. Extended krylov subspaces: approximation of the matrix square root and related functions. *SIAM Journal on Matrix Analysis and Applications*, 19(3):755–771, 1998.
- [10] H. El Kahza, W. Taitano, J.-M. Qiu, and L. Chacón. Krylov-based adaptive-rank implicit time integrators for stiff problems with application to nonlinear fokker-planck kinetic models. *Journal of Computational Physics*, 518:113332, 2024.
- [11] G. H. Golub and C. F. Van Loan. *Matrix computations*. JHU press, 2013.
- [12] W. Guo, J. F. Ema, and J.-M. Qiu. A local macroscopic conservative (lomac) low rank tensor method with the discontinuous galerkin method for the vlasov dynamics. *Communications on Applied Mathematics and Computation*, pages 1–26, 2023.
- [13] W. Guo and J.-M. Qiu. A low rank tensor representation of linear transport and nonlinear vlasov solutions and their associated flow maps. *Journal of Computational Physics*, 458:111089, 2022.
- [14] W. Guo and J.-M. Qiu. A conservative low rank tensor method for the vlasov dynamics. *SIAM Journal on Scientific Computing*, 2024.
- [15] Y. Hao and V. Simoncini. The sherman–morrison–woodbury formula for generalized linear matrix equations and applications. *Numerical linear algebra with applications*, 28(5):e2384, 2021.
- [16] D. A. Knoll and D. E. Keyes. Jacobian-free newton–krylov methods: a survey of approaches and applications. *Journal of Computational Physics*, 193(2):357–397, 2004.
- [17] O. Koch and C. Lubich. Dynamical low-rank approximation. *SIAM Journal on Matrix Analysis and Applications*, 29(2):434–454, 2007.
- [18] K. Kormann. A semi-Lagrangian Vlasov solver in tensor train format. *SIAM Journal on Scientific Computing*, 37(4):B613–B632, 2015.
- [19] O. Koshkarov and L. Chacón. A fully implicit, asymptotic-preserving, semi-lagrangian algorithm for the time dependent anisotropic heat transport equation. *Journal of Computational Physics*, 519:113381, 2024.
- [20] D. Kressner and C. Tobler. Krylov subspace methods for linear systems with tensor product structure. *SIAM journal on matrix analysis and applications*, 31(4):1688–1714, 2010.
- [21] H. Y. Lam, G. Ceruti, and D. Kressner. Randomized low-rank runge-kutta methods. *arXiv preprint arXiv:2409.06384*, 2024.
- [22] C. Lubich and I. V. Oseledets. A projector-splitting integrator for dynamical low-rank approximation. *BIT Numerical Mathematics*, 54(1):171–188, 2014.

- [23] S. Meng, D. Appelo, and Y. Cheng. Preconditioning low rank generalized minimal residual method (gmres) for implicit discretizations of matrix differential equations. *arXiv preprint arXiv:2410.07465*, 2024.
- [24] J. Nakao, J.-M. Qiu, and L. Einkemmer. Reduced augmentation implicit low-rank (rail) integrators for advection-diffusion and fokker-planck models. *arXiv preprint arXiv:2311.15143*, 2023.
- [25] D. Palitta and V. Simoncini. Matrix-equation-based strategies for convection–diffusion equations. *BIT Numerical Mathematics*, 56:751–776, 2016.
- [26] D. Palitta and V. Simoncini. Optimality properties of galerkin and petrov–galerkin methods for linear matrix equations. *Vietnam Journal of Mathematics*, 48(4):791–807, 2020.
- [27] C. E. Powell, D. Silvester, and V. Simoncini. An efficient reduced basis solver for stochastic galerkin matrix equations. *SIAM Journal on Scientific Computing*, 39(1):A141–A163, 2017.
- [28] A. Quarteroni, R. Sacco, and F. Saleri. *Numerical mathematics*, volume 37. Springer Science & Business Media, 2006.
- [29] A. Rodgers and D. Venturi. Implicit integration of nonlinear evolution equations on tensor manifolds. *Journal of Scientific Computing*, 97(2):33, 2023.
- [30] Y. Saad. Numerical solution of large lyapunov equations. Technical report, 1989.
- [31] S. D. Shank and V. Simoncini. Krylov subspace methods for large-scale constrained sylvester equations. *SIAM Journal on Matrix Analysis and Applications*, 34(4):1448–1463, 2013.
- [32] S. D. Shank, V. Simoncini, and D. B. Szyld. Efficient low-rank solution of generalized lyapunov equations. *Numerische Mathematik*, 134(2):327–342, 2016.
- [33] V. Simoncini. A new iterative method for solving large-scale lyapunov matrix equations. *SIAM Journal on Scientific Computing*, 29(3):1268–1288, 2007.
- [34] V. Simoncini and Y. Hao. Analysis of the truncated conjugate gradient method for linear matrix equations. *SIAM Journal on Matrix Analysis and Applications*, 44(1):359–381, 2023.